Numerical simulation of piecewise-linear models of gene regulatory networks using complementarity systems

Vincent Acary *, Hidde de Jong, Bernard Brogliato

INRIA Grenoble - Rhône-Alpes, 655 avenue de l'Europe, 38330, Montbonnot, France

HIGHLIGHTS

- An equivalence result between the Filippov and Aizerman–Pyatnitskii (AP) extensions.
- The reformulation of the AP-extension as a Complementarity System (CS).
- A theoretically sound and practically useful numerical simulation method.
- A time-integration method for the resulting CS with sliding motions.
- Illustration of the interest by an analysis of three synthetic networks.

ARTICLE INFO

ABSTRACT

Gene regulatory networks control the response of living cells to changes in their environment. A class of piecewise-linear (PWL) models, which capture the switch-like interactions between genes by means of step functions, has been found useful for describing the dynamics of gene regulatory networks. The step functions lead to discontinuities in the right-hand side of the differential equations. This has motivated extensions of the PWL models based on differential inclusions and Filippov solutions, whose analysis requires sophisticated numerical tools. We present a method for the numerical analysis of one proposed extension, called Aizerman–Pyatnitskii (AP)-extension, by reformulating the PWL models as a mixed complementarity system (MCS). This allows the application of powerful methods developed for this class of nonsmooth dynamical systems, in particular those implemented in the Siconos platform. We also show that under a set of reasonable biological assumptions, putting constraints on the right-hand side of the PWL models, AP-extensions and classical Filippov (F)-extensions are equivalent. This means that the proposed numerical method is valid for a range of different solution concepts. We illustrate the practical interest of our approach through the numerical analysis of three well-known networks developed in the field of synthetic biology.

© 2013 Elsevier B.V. All rights reserved.

1. Introduction

When confronted with changing environmental conditions, living systems have a remarkable capacity to rapidly adapt their functioning. For instance, the response of a bacterial cell to the depletion of an essential nutrient leads to the upregulation and downregulation of the expression of up to several hundreds of genes [1]. The genes encode enzymes, transcription regulators, membrane transporters and other macromolecules playing a role in cellular processes. The control of the adjustment of gene expression levels is achieved by so-called *gene regulatory networks*, consisting of genes, RNAs, proteins, and their mutual regulatory interactions.

In order to understand how a particular network structure brings about observed changes in gene expression, mathematical models in combination with computer simulation are increasingly used, especially in the emerging field of systems biology [2]. The modeling of gene regulatory networks also plays a prominent role in synthetic biology, which aims at designing a network structure capable of producing a desired gene expression pattern, for instance a robust oscillation or an externally controlled switch [3]. The networks may be constructed *de novo* or obtained by rewiring a natural regulatory network.

A variety of formalisms are available for modeling gene regulatory networks [4,5]. For many purposes, approximate models based on simplifications of classical kinetic models have been proven useful [6–8]. First, the approximate models are easier to calibrate against experimental data, due to the fact that they reduce the number of parameters and the complexity of the rate equations. This may help relieve what is currently a bottleneck for modeling in systems biology, namely obtaining reliable estimates

---

* Corresponding author. Tel.: +33 476 615 229; fax: +33 476 615 455.
E-mail address: vincent.acary@inria.fr (V. Acary).

of parameter values. Second, the simplified mathematical form of the models makes them easier to analyze. Among other things, this makes it possible to single out the precise role of specific subnetworks [9,10] and to analyze the feasibility of control schemes [11].

In this paper we look at one particular class of approximate models of gene regulatory networks, so-called *piecewise-linear (PWL) models* [12]. The PWL models are systems of coupled differential equations in which the variables denote concentrations of gene products, typically proteins. The rate of change of a concentration at a particular time-point may be regulated by other proteins through direct or indirect interactions. The PWL models capture these regulatory effects by means of step functions that change their value in a switch-like manner at threshold concentrations of the regulatory proteins. The step functions are approximations of the sigmoidal response functions often found in gene regulation.

PWL models with step functions have favorable mathematical properties, which allows for the analysis of steady states, limit cycles, and their stability [13–16]. The use of step functions, however, leads to discontinuities in the right-hand side of the differential equations, due to the abrupt changes of the value of a step function at its threshold. These discontinuities are sometimes ignored, which is potentially dangerous as it may cause steady states and other important dynamical properties of the system to be missed. In order to deal with the discontinuities, several authors have proposed the use of differential inclusions and Filippov solutions [17–19]. These proposals to extend PWL models to differential inclusions differ in subtle but nontrivial ways, giving rise to systems with nonequivalent dynamics [19,20].

Currently, only few computational tools are available to support the analysis of the differential inclusions obtained from Filippov extensions of PWL models. Genetic Network Analyzer (GNA) provides a qualitative analysis of PWL models of gene regulatory networks (*e.g.*, [21,22]). However, the analysis is based on hyperrectangular overapproximations of the differential inclusions proposed in [17], and it is currently not clear to which extent this introduces artifacts in the analysis. Moreover, the predictions obtained from this analysis are purely qualitative, describing possible transitions between state-space regions rather than giving numerical solutions. Alternatively, an algorithm based on the use of steep sigmoidal response functions in combination with singular perturbation theory has been presented [23,24].

The aim of this paper is to propose a theoretically sound and practically useful method for the numerical simulation of gene regulatory networks described by PWL models. We notably show that the Aizerman & Pyatnitskii extension (see [17, Definition c, page 55] or [25]) of PWL models can be reformulated in the framework of complementarity systems or differential variational inequalities [26–28]. The Aizerman & Pyatnitskii extension has been introduced in the context of PWL models of gene regulatory networks in [19,20], where it is shown that it leads to a more restrictive extension than the standard Filippov extension. The reformulation as a complementarity system allows us to employ the rich store of numerical methods available for these and other classes of discontinuous systems [26,29]. Moreover, we show that under two reasonable biological assumptions, posing constraints on the admissible network structures, the different extensions of PWL models that have been proposed, as well as the hyperrectangular overapproximation in [22], are equivalent. This means that the numerical simulation approach developed in this paper is valid for a range of different solution concepts for PWL models of gene regulatory networks.

We illustrate the interest of our numerical simulation approach by means of the analysis of three synthetic networks published in the literature: the repressilator [30], an oscillator with positive feedback [31], and the IRMA network [32]. We develop PWL models of these networks, either from scratch or by adapting existing ODE models, and numerically simulate the dynamic response of these networks to external stimuli. The simulations are shown to reproduce known qualitative features of these networks, notably the capability to generate (damped) oscillations for the first two networks, and a switch-on/switch-off response after a change in the growth medium for the third. We believe these examples demonstrate that the numerical simulation approach developed in this paper provides a useful extension of the toolbox of modelers of gene regulatory networks.

2. PWL models of gene regulatory networks

2.1. Definition of PWL models

The dynamics of genetic regulatory networks can be described by piecewise-linear (PWL) differential equation models using step functions to account for regulatory interactions [12,33,34]. In this section we briefly summarize the PWL modeling framework.

We denote by $x = (x_1, \ldots, x_n)^T \in \Omega$ a vector of cellular protein or RNA concentrations, where $\Omega \subset \mathbb{R}^n_+$ is a bounded n-dimensional hyperrectangular subset of $\mathbb{R}^n_+$. For each concentration variable x_i, $i \in \{1, \ldots, n\}$, we distinguish a set of constant, strictly positive threshold concentrations $\{\theta_i^1, \ldots, \theta_i^{p_i}\}$, $p_i > 0$. At its thresholds a protein may affect the expression of genes encoding other proteins or the expression of its own gene. We call $\Theta = \bigcup_{i \in \{1, \ldots, n\}, k \in \{1, \ldots, p_i\}} \{x \in \Omega \mid x_i = \theta_i^k\}$ the subset of Ω defined by the threshold hyperplanes.

Definition 1 (*PWL Model*). A PWL model of a gene regulatory network is defined by a set of coupled differential equations

$$\dot{x}_i = f_i(x) = -\gamma_i x_i + b_i(x)$$
$$= -\gamma_i x_i + \sum_{l \in L_i} \kappa_i^l b_i^l(x), \quad i \in \{1, \ldots, n\}, \tag{1}$$

where κ_i^l and γ_i are positive synthesis and degradation constants, respectively, $L_i \subset \mathbb{N}$ are sets of indices of regulation terms, and $b_i^l : \Omega \setminus \Theta \to \{0, 1\}$ are so-called regulation functions.

Intuitively, (1) defines the rate of change of each concentration x_i as the difference of the rate of synthesis (the second term in the right-hand side) and the rate of degradation (the first term). The synthesis term depends on the concentrations of regulatory proteins through the regulation functions, which account for the interactions between the genes in the network. Degradation is described by a first-order term including contributions of growth dilution and protein degradation. While this is sufficient for the examples treated in this paper, the degradation term in (1) can be easily extended to include proteolytic regulators.

Each regulation function $b_i^l(\cdot)$ is defined in terms of *step functions*

$$s^+(x_j, \theta_j^k) = \begin{cases} 1 & \text{if } x_j > \theta_j^k \\ 0 & \text{if } x_j < \theta_j^k \end{cases} \quad \text{and}$$

$$s^-(x_j, \theta_j^k) = \begin{cases} 0 & \text{if } x_j > \theta_j^k \\ 1 & \text{if } x_j < \theta_j^k, \end{cases} \tag{2}$$

where x_j is a concentration variable, $j \in \{1, \ldots, n\}$, and θ_j^k a threshold for x_j, $k \in \{1, \ldots, p_i\}$. Notice that $s^-(x_j, \theta_j^k) = 1 - s^+(x_j, \theta_j^k)$. The step functions capture the switch-like character of gene regulation by transcription factors and other proteins. The regulation functions are algebraic equivalents of discrete Boolean functions expressing the combinatorial logic of gene regulation [35].

For future use, we introduce the following generalizations of the step functions $s^+(x_j, \theta_j^k)$ and $s^-(x_j, \theta_j^k)$, which consists of extending the function at the discontinuities:

$$S^+(x_j, \theta_j^k) = \begin{cases} 1 & x_j > \theta_j^k \\ [0, 1] & x_j = \theta_j^k \\ 0 & x_j < \theta_j^k \end{cases} \quad \text{and}$$

$$S^-(x_j, \theta_j^k) = \begin{cases} 0 & x_j > \theta_j^k \\ [0, 1] & x_j = \theta_j^k \\ 1 & x_j < \theta_j^k. \end{cases} \tag{3}$$

Fig. 1 gives an example of a PWL model of a simple two-gene network. The network consists of two genes each of which encodes a protein that inhibits the expression of its own gene and activates the expression of the other gene. Activation and inhibition are assumed to occur at different thresholds. In order for a gene to be expressed, its activator needs to be present (above its threshold) and its inhibitor absent (below its threshold). While this example is used for illustrative purposes in this and the next section, it should be noted that it includes many aspects of actual regulatory networks: auto-regulation, cross-regulation, and combinatorial regulation of gene expression (see Section 6). Several PWL models of actual regulatory networks are available in the literature, see [36] and references therein.
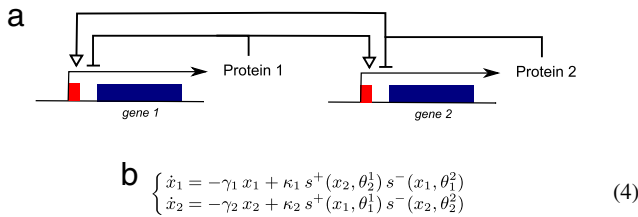

Fig. 1. (a) Example of a gene regulatory network of two genes, each coding for a regulatory protein. (b) PWL model corresponding to the network in (a).

$$\begin{cases} \dot{x}_1 = -\gamma_1 x_1 + \kappa_1 s^+(x_2, \theta_2^1) s^-(x_1, \theta_1^2) \\ \dot{x}_2 = -\gamma_2 x_2 + \kappa_2 s^+(x_1, \theta_1^1) s^-(x_2, \theta_2^2) \end{cases} \tag{4}$$

2.2. Regulation functions in PWL models

Which regulation functions $b_i^l(\cdot)$ entering the PWL models are admissible? In order to answer this question, we first develop how the regulation functions relate to Boolean functions describing the combinatorial control of gene regulation.

Recall that each variable x_j has p_j thresholds $\{\theta_j^1, \ldots, \theta_j^{p_j}\}$. The step functions can be associated with Boolean variables X_j^k such that

$$\begin{aligned} X_j^k(x) = (x_j > \theta_j^k) = s^+(x_j, \theta_j^k) \\ \bar{X}_j^k(x) = (x_j < \theta_j^k) = s^-(x_j, \theta_j^k), \end{aligned} \tag{5}$$

where $\bar{X}$ denotes the complemented variable of X.

Let us give some basic definitions of Boolean algebra [37, Chapter 3]. A literal denoted by $\mathcal{Y}_j$ is defined either as the Boolean variable Y_j or its negation $\bar{Y}_j$. Given a set of n Boolean variables $Y_1, \ldots, Y_n$, a minterm m is defined as a conjunction of exactly n literals in which each $\mathcal{Y}_j, j \in \{1 \ldots n\}$ appears once (each variable appears once in either its complemented or uncomplemented form). That is,

$$m = \prod_{j=1}^{n} \mathcal{Y}_j. \tag{6}$$

For the set of variables $X_j^k, j \in \{1, \ldots, n\}, k \in \{1, \ldots, p_j\}$, we have 2^p minterms, with $p = \sum_{j \in \{1, \ldots, n\}} p_j$, and these are denoted as

$$m_\alpha(x) = \prod_{j=1}^{n} \prod_{k=1}^{p_j} \mathcal{X}_j^k(x), \quad \alpha \in \{0, \ldots, 2^p - 1\}. \tag{7}$$

The subscript α corresponds to the decimal equivalent of the conventional binary encoding of literals (1 for X_j^k and 0 for $\bar{X}_j^k$). Table 1 gives an example of the minterms for the four variables in the example of Fig. 1, with their corresponding binary encoding and decimal equivalent.

Regulation functions can now be defined as the minterm expression of a Boolean function [38]. More precisely, they can be rewritten in the minterm disjunctive normal form (DNF):

$$b_i^l(x) = \sum_{\alpha=0}^{2^p - 1} c_{i,\alpha}^l m_\alpha(x), \tag{8}$$

with $c_{i,\alpha}^l \in \{0, 1\}$. By means of (8), the PWL models can be written as

$$\dot{x}_i = f_i(x) = -\gamma_i x_i + \sum_{l \in L_i} \kappa_i^l \sum_{\alpha=0}^{2^p - 1} c_{i,\alpha}^l m_\alpha(x), \quad i \in \{1, \ldots, n\}. \tag{9}$$

As an example, consider the DNF of the regulation functions in the PWL model of Fig. 1. Since $L_1 = L_2 = 1$, we omit the superscript l for κ_i^l and $c_{i,\alpha}^l$. As each variable has two thresholds, the canonical representation is composed of the 16 minterms shown in Table 1. Notice that for each state variable x_1, x_2, only 4 of the coefficients $c_{i,\alpha}$ equal 1. We thus obtain the following PWL model:

$$\begin{cases} \dot{x}_1 = -\gamma_1 x_1 + \kappa_1 \sum_{\alpha=0}^{15} c_{1,\alpha} m_\alpha(x) \\ \dot{x}_2 = -\gamma_2 x_2 + \kappa_2 \sum_{\alpha=0}^{15} c_{2,\alpha} m_\alpha(x), \end{cases} \tag{10}$$

with

$$\begin{cases} c_{1,2} = c_{1,3} = c_{1,10} = c_{1,11} = 1 \\ c_{2,8} = c_{2,10} = c_{2,12} = c_{2,14} = 1 \\ c_{1,\alpha} = c_{2,\alpha} = 0 \quad \text{otherwise.} \end{cases} \tag{11}$$

Writing out the right-hand side of (10) yields

$$\begin{cases} \dot{x}_1 = -\gamma_1 x_1 + \kappa_1 (m_2(x) + m_3(x) + m_{10}(x) + m_{11}(x)) \\ \dot{x}_2 = -\gamma_2 x_2 + \kappa_2 (m_8(x) + m_{10}(x) + m_{12}(x) + m_{14}(x)), \end{cases} \tag{12}$$

which can be easily simplified to (4) by noting that $s^+(x_2, \theta_2^2) = 1 - s^-(x_2, \theta_2^2)$ and $s^+(x_1, \theta_1^1) = 1 - s^-(x_1, \theta_1^1)$. More generally, minimization procedures from the field of circuit design and finite automata theory [37, Chapter 4] can be used to reduce the canonical representation to polynomials that are simpler to handle in practice.

The definition of regulation functions in DNF motivates the following modeling assumption [19].

Assumption 2. The regulation functions $b_i^l(\cdot)$ are multi-affine functions, that is, they are affine with respect to each $s^+(x_j, \theta_j^k)$, for $j \in \{1, \ldots, n\}$ and $k \in \{1, \ldots, p_j\}$.

This assumption can be shown to be generic for all regulation functions corresponding to Boolean functions written in DNF.

Proposition 3. All PWL models (1) with regulation functions $b_i^l(\cdot)$ in DNF satisfy Assumption 2.

The proposition directly follows from the observation that the regulation functions in (9) are sums of minterms, each of which is affine with respect to the step functions $s^+(x_j, \theta_j^k)$, bearing in mind that $s^-(x_j, \theta_j^k) = 1 - s^+(x_j, \theta_j^k)$.

A second assumption requires that, when two genes have a common regulation, the latter does not act upon the two genes at the same threshold [39].

Table 1
Minterms and their binary encoding for the PWL model in Fig. 1.

Binary encoding				Decimal equivalent	Minterm	Constant
$\mathcal{X}_1^1$	$\mathcal{X}_1^2$	$\mathcal{X}_2^1$	$\mathcal{X}_2^2$	α	$m_\alpha(x)$	c_α
0	0	0	0	0	$s^-(x_1,\theta_1^1)\,s^-(x_1,\theta_1^2)\,s^-(x_2,\theta_2^1)\,s^-(x_2,\theta_2^2)$	c_0
0	0	0	1	1	$s^-(x_1,\theta_1^1)\,s^-(x_1,\theta_1^2)\,s^-(x_2,\theta_2^1)\,s^+(x_2,\theta_2^2)$	c_1
0	0	1	0	2	$s^-(x_1,\theta_1^1)\,s^-(x_1,\theta_1^2)\,s^+(x_2,\theta_2^1)\,s^-(x_2,\theta_2^2)$	c_2
0	0	1	1	3	$s^-(x_1,\theta_1^1)\,s^-(x_1,\theta_1^2)\,s^+(x_2,\theta_2^1)\,s^+(x_2,\theta_2^2)$	c_3
0	1	0	0	4	$s^-(x_1,\theta_1^1)\,s^+(x_1,\theta_1^2)\,s^-(x_2,\theta_2^1)\,s^-(x_2,\theta_2^2)$	c_4
0	1	0	1	5	$s^-(x_1,\theta_1^1)\,s^+(x_1,\theta_1^2)\,s^-(x_2,\theta_2^1)\,s^+(x_2,\theta_2^2)$	c_5
0	1	1	0	6	$s^-(x_1,\theta_1^1)\,s^+(x_1,\theta_1^2)\,s^+(x_2,\theta_2^1)\,s^-(x_2,\theta_2^2)$	c_6
0	1	1	1	7	$s^-(x_1,\theta_1^1)\,s^+(x_1,\theta_1^2)\,s^+(x_2,\theta_2^1)\,s^+(x_2,\theta_2^2)$	c_7
1	0	0	0	8	$s^+(x_1,\theta_1^1)\,s^-(x_1,\theta_1^2)\,s^-(x_2,\theta_2^1)\,s^-(x_2,\theta_2^2)$	c_8
1	0	0	1	9	$s^+(x_1,\theta_1^1)\,s^-(x_1,\theta_1^2)\,s^-(x_2,\theta_2^1)\,s^+(x_2,\theta_2^2)$	c_9
1	0	1	0	10	$s^+(x_1,\theta_1^1)\,s^-(x_1,\theta_1^2)\,s^+(x_2,\theta_2^1)\,s^-(x_2,\theta_2^2)$	c_{10}
1	0	1	1	11	$s^+(x_1,\theta_1^1)\,s^-(x_1,\theta_1^2)\,s^+(x_2,\theta_2^1)\,s^+(x_2,\theta_2^2)$	c_{11}
1	1	0	0	12	$s^+(x_1,\theta_1^1)\,s^+(x_1,\theta_1^2)\,s^-(x_2,\theta_2^1)\,s^-(x_2,\theta_2^2)$	c_{12}
1	1	0	1	13	$s^+(x_1,\theta_1^1)\,s^+(x_1,\theta_1^2)\,s^-(x_2,\theta_2^1)\,s^+(x_2,\theta_2^2)$	c_{13}
1	1	1	0	14	$s^+(x_1,\theta_1^1)\,s^+(x_1,\theta_1^2)\,s^+(x_2,\theta_2^1)\,s^-(x_2,\theta_2^2)$	c_{14}
1	1	1	1	15	$s^+(x_1,\theta_1^1)\,s^+(x_1,\theta_1^2)\,s^+(x_2,\theta_2^1)\,s^+(x_2,\theta_2^2)$	c_{15}

Assumption 4. Every step function $s^+(x_j,\theta_j^k)$, with $j \in \{1,\ldots,n\}$ and $k \in \{1,\ldots,p_j\}$, occurs in at most one $b_i(\cdot)$, $i \in \{1,\ldots,n\}$. As a consequence, for a given j,k, every vector $[\partial b_i(x)/\partial s_{jk}^+]_{i\in\{1,\ldots,n\}}$, with $s_{jk}^+ \equiv s^+(x_j,\theta_j^k)$, has at most one non-zero element.

Assumption 4 is a rather weak modeling assumption, in the sense that there is usually no compelling biological reason for two genes to be regulated at exactly the same threshold. The notable exception is the case of bacterial genes co-transcribed from the same promoter, that is, genes that are included in the same operon. Notice that all models of biological networks presented in Section 6 satisfy Assumption 4.

The interest of the above restrictions on regulation functions, and thus on the right-hand sides of the PWL models, is that together they entail the equivalency of different solution concepts. This will be shown in the next section.

3. Solutions of PWL models

3.1. Filippov extensions of PWL models

The use of step functions $s^\pm(x_j,\theta_j^k)$ in (9) gives rise to mathematical complications, because the step functions are undefined and discontinuous at $x_j = \theta_j^k$. Therefore, $f(\cdot) = (f_1(\cdot),\ldots,f_n(\cdot))^T$ is undefined and may be discontinuous on the threshold hyperplanes Θ. In order to deal with this problem, we can follow an approach originally proposed by Filippov [17] and widely used in control theory. It consists in extending the differential equation $\dot{x} = f(x)$, $x \in \Omega \setminus \Theta$, to a differential inclusion. Following the book of Filippov, Machina and Ponosov [19] review several different ways in which this can be done (see also [20,40]). Below we discuss the two main alternatives, which we call F- and AP-extensions, respectively, and we give precise definitions of the corresponding solutions of the PWL models.

Definition 5 (*F-extension of PWL Models*)**.** The F-extension of the PWL model (1) is defined by the differential inclusion

$$\dot{x} \in \mathbf{F}(x), \quad \text{with } \mathbf{F}(x) = \overline{co}\left(\left\{\lim_{y\to x,\, y\notin\Theta} f(y)\right\}\right), \quad x \in \Omega, \qquad (13)$$

where $\overline{co}(P)$ denotes the closed convex hull of the set P, and $\{\lim_{y\to x,\, y\notin\Theta} f(y)\}$ the set of all limit values of $f(y)$, for $y \notin \Theta$ and $y \to x$.

This definition corresponds to the classical Filippov approach [17], as applied in the context of gene regulatory network modeling in [18].

Formally, we define a *F-PWL system* Σ as the triple $(\Omega, \Theta, \mathbf{F})$, that is, the set-valued function $\mathbf{F}(\cdot)$ given by (13), defined on the n-dimensional state space Ω, with Θ the union of the threshold hyperplanes [22].

Definition 6. A solution of an F-PWL system Σ on a time interval I is a solution of the differential inclusion (13) on I, that is, an absolutely-continuous vector-valued function $\xi(\cdot)$ such that $\dot{\xi}(t) \in \mathbf{F}(\xi(t))$ almost everywhere on I.

For all $x_0 \in \Omega$ and $\tau \in \mathbb{R}_+ \cup \{\infty\}$, $\Xi_\Sigma(x_0,\tau)$ denotes the set of solutions $\xi(t)$ of the PWL system Σ, for the initial condition $\xi(0) = x_0$, and $t \in [0,\tau]$. In particular, notice that the derivative of $\xi(\cdot)$ may not exist, and therefore $\dot{\xi}(t) \in \mathbf{F}(\xi(t))$ may not hold, if ξ reaches or leaves Θ at t. The existence of at least one solution ξ on some time interval $[0,\tau]$, $\tau > 0$, with initial condition $\xi(0) = x_0$ is guaranteed for all $x_0 \in \Omega$ [17]. However, in general there is not a unique solution.

As stated above, the book of Filippov proposes other extensions of the PWL systems, which do not define the right-hand side of the inclusion as the limit values of the function $f(y)$, like in (13). A common definition of the right-hand side, following [17, Definition c), page 55], is attributed to [25] for systems of the form

$$\dot{x} = f(x,u), \quad x \in \mathbb{R}^n, \, u \in \mathbb{R}^p, \qquad (14)$$

where the function $f : \mathbb{R}^{n+p} \to \mathbb{R}^n$ is continuous in the set of arguments and $u(x) : \mathbb{R}^n \to \mathbb{R}^p$ is discontinuous. Systems (14) are often encountered in control theory, especially in variable structure systems and sliding mode control [41–43]. At the point of discontinuity, for $i \neq j$, the arguments u_i and u_j of f are supposed to vary independently on the sets $U_i(x)$ and $U_j(x)$, usually assumed to be closed convex sets in $\mathbb{R}$. The right-hand side of the differential inclusion in the sense of Aizerman and Pyatnitskii is then defined as

$$\mathbf{G}(x) = \left\{y \mid y = f(x,u),\, u_i \in U_i(x),\, i \in \{1\ldots p\}\right\}. \qquad (15)$$

The set-valued vector field $\mathbf{G}(x)$ is generically non-convex and therefore often replaced by its convexification $\mathbf{H}(x) = \overline{co}(\mathbf{G}(x))$. A standard result states that if $f(\cdot)$ in (14) is linear in u, then $\mathbf{G}(x) = \mathbf{H}(x)$ if all U_i, $i \in \{1,\ldots,m\}$, are convex [17, page 56] and [43]. Furthermore, if the arguments u_i, $i \in \{1,\ldots,p\}$, are discontinuous on surfaces S_i, such that the surfaces are different and the normal vectors at the points of intersection are not linearly dependent, then $\mathbf{F}(x) = \mathbf{G}(x) = \mathbf{H}(x)$.

In the context of the modeling of gene regulatory networks, Machina and Ponosov [19] apply the alternative extension **G** of the PWL models, using the generalized step functions $S^+(x_j, \theta_j)$ and $S^-(x_j, \theta_j)$ (Section 2.1) instead of the set-valued functions U_i. They argue that this extension gives results that are closer to those obtained with gene regulatory network models using sigmoidal functions rather than step functions, in the limit of infinitely-steep sigmoids [24,39]. Moreover, as we will show below, this definition is more convenient for numerical simulation purposes. We call the resulting differential inclusion the *Aizerman–Pyatnitskii (AP)-extension* of PWL models.[1]

Remark 7. In the seminal book of Filippov [17], $\mathbf{G}(\cdot)$ is denoted as $F_1(\cdot)$ and $\mathbf{H}(\cdot)$ as $F_2(\cdot)$. In order to avoid confusion with the components of $\mathbf{F}(\cdot)$, we choose the alternative notation proposed here.

Let $\sigma = (\sigma_1^1, \ldots, \sigma_1^{p_1}, \ldots, \sigma_n^1, \ldots, \sigma_n^{p_n})^T \in [0, 1]^p$. Moreover, define the function $g : \mathbb{R}^p \to \mathbb{R}^n$ by

$$g_i(\sigma) = \sum_{l \in L_n} \kappa_i^l \, \tilde{b}_i^l(\sigma), \quad j \in \{1, \ldots, n\}, \tag{16}$$

where $\tilde{b}_i^l(\cdot)$ are obtained from $b_i^l(\cdot)$ by replacing every occurrence of $s^+(x_j, \theta_j^k)$ and $s^-(x_j, \theta_j^k)$ by σ_j^k and $1 - \sigma_j^k$, respectively, for all $j \in \{1, \ldots, n\}$ and $k \in \{1, \ldots, p_j\}$.

Definition 8 (*AP-extension of PWL Models*)**.** The AP-extension of a PWL model (1) is defined by the following differential inclusion

$$\dot{x} \in \begin{bmatrix} \mathbf{G}_1(x) \\ \vdots \\ \mathbf{G}_n(x) \end{bmatrix} = \left\{ \begin{bmatrix} -\gamma_1 x_1 + g_1(\sigma) \\ \vdots \\ -\gamma_n x_n + g_n(\sigma) \end{bmatrix} \middle| \sigma_j^k \in S^+(x_j, \theta_j^k), \right.$$
$$\left. j \in \{1, \ldots, n\}, \, k \in \{1, \ldots, p_j\} \right\}. \tag{17}$$

In line with this definition, we obtain an *AP-PWL system P* given by the triple $(\Omega, \Theta, \mathbf{G})$. The solutions of this system are defined as follows.

Definition 9. A solution of an AP-PWL system P on a time interval I is a solution of the differential inclusion (17) on I, that is, an absolutely-continuous vector-valued function $\xi(\cdot)$ such that $\dot{\xi}(t) \in \mathbf{G}(\xi(t))$ almost everywhere on I.

The set of solutions of the AP-PWL system P is denoted by $\Xi_P(x_0, \tau)$, for $\xi(0) = x_0$, and $t \in [0, \tau]$. Since $\mathbf{G}(\cdot)$ may not be convex contrary to $\mathbf{F}(\cdot)$, the existence of solutions of this system for every $x_0 \in \Omega$ cannot be guaranteed in general (for two-dimensional systems existence has been proven [20]).

Notice that the definition of the AP-extension requires that all occurrences of a step function $s^+(x_j, \theta_j^k)$ in (17) are replaced by the same value $\sigma_j^k \in S^+(x_j, \theta_j^k)$, and all occurrences of $s^-(x_j, \theta_j^k)$ by the same value $1 - \sigma_j^k$. In other words, all occurrences of a step function $s^+(x_j, \theta_j^k)$ (respectively $s^-(x_j, \theta_j^k)$) are replaced by a selection σ_j^k (respectively $1 - \sigma_j^k$). From a modeling point of view this makes sense, as the different occurrences in $b(\cdot)$ of the step function $s^{\pm}(x_j, \theta_j^k)$ usually correspond to a single underlying biophysical process. However, from a mathematical point of view

one could imagine to relax the definition by allowing different values $\sigma_j^k \in S^+(x_j, \theta_j^k)$ for different occurrences of $s^+(x_j, \theta_j^k)$, and by decoupling the values for positive and negative step functions. This corresponds to replacing (15) by the alternative definition $\hat{\mathbf{G}}(x) = f(x, U(x))$, where $U(x) = [U_i(x)]_{i \in \{1,\ldots,p\}}^T$. In the Appendix we show that, in general, this notation is ambiguous and leads to an extension of the PWL systems that is not equivalent with Definition 8. This ambiguity is discussed in [43, Section 1.3], where two inputs u_i and u_j in a controlled system of the form (14) are subjected to discontinuities over the same surface $S_i = S_j$.

3.2. Relations between different Filippov extensions of PWL models

The natural question to ask is how the solutions of the F-PWL system given by the differential inclusions (13) relate to the solutions of the AP-PWL system given by (17). This means that we have to compare $\mathbf{F}(\cdot)$ and $\mathbf{G}(\cdot)$.

Proposition 10. *Under Assumption 2,* $\mathbf{F}(x) = \overline{co}(\mathbf{G}(x))$ *for all* $x \in \Omega$.

This result has been proven in [19]. Since in general $\mathbf{G}(x)$ is not a convex set ($\mathbf{G}(x) \neq \overline{co}(\mathbf{G}(x))$), it follows from the proposition that the two solution concepts may give different results. We illustrate this by means of the following example from [19]:

$$\begin{cases} \dot{x}_1 = -\gamma_1 x_1 + \kappa_1 \, [s^+(x_1, \theta_1) + s^+(x_2, \theta_2) \\ \qquad - 2 \, s^+(x_1, \theta_1) \, s^+(x_2, \theta_2)] \\ \dot{x}_2 = -\gamma_2 x_2 + \kappa_2 \, [1 - s^+(x_1, \theta_1) \, s^+(x_2, \theta_2)]. \end{cases} \tag{18}$$

Consider this PWL system at the intersection of the two thresholds, that is, at $x = (\theta_1, \theta_2)^T$. According to Definition 5, we have

$$\mathbf{F}(x) = \begin{bmatrix} -\gamma_1 x_1 \\ -\gamma_2 x_2 \end{bmatrix} + \overline{co} \left\{ \begin{bmatrix} 0 \\ 0 \end{bmatrix}, \begin{bmatrix} 0 \\ \kappa_2 \end{bmatrix}, \begin{bmatrix} \kappa_1 \\ \kappa_2 \end{bmatrix} \right\}, \tag{19}$$

that is, the convex combination of the vector fields in the four regions having $(\theta_1, \theta_2)^T$ in their boundary, evaluated at this point. Notice that the vector fields in the regions $\{x_1 > \theta_1, x_2 < \theta_2\}$ and $\{x_1 < \theta_1, x_2 > \theta_2\}$ are the same ($[-\gamma_1 x_1 + k_1, -\gamma_2 x_2 + k_2]^T$), which explains that only three (instead of four) vectors appear in (19). Fig. 2(a) shows the convex envelope of the vector fields at the intersection of the thresholds, for the case that $\kappa_1 > \gamma_1 \theta_1$ and $\kappa_2 > \gamma_2 \theta_2$.

The AP-extension of the PWL model (18), according to Definition 8, is defined as follows:

$$\mathbf{G}(x) = \left\{ \begin{bmatrix} -\gamma_1 x_1 + \kappa_1 \, [\sigma_1 + \sigma_2 - 2\sigma_1 \sigma_2] \\ -\gamma_2 x_2 + \kappa_2 \, [1 - \sigma_1 \sigma_2] \end{bmatrix} \middle| \sigma_1, \sigma_2 \in [0, 1] \right\}. \tag{20}$$

As can be seen in Fig. 2(b), $\mathbf{G}(x)$ is not equal to $\mathbf{F}(x)$ at $x = (\theta_1, \theta_2)^T$. The vertices of $\mathbf{F}(x)$ are included in $\mathbf{G}(x)$, where they correspond to the cases that σ_1 and σ_2 take their extreme values 0 or 1, as shown in the figure. However, $\mathbf{G}(x)$ is a strict subset of $\mathbf{F}(x)$ and is not convex.

The example shows that the different Filippov extensions are not equivalent, but the question can be posed if differences occur when analyzing biologically relevant network structures. For example, the network represented by the PWL model (18) consists of two regulators that jointly regulate their own genes, at exactly the same threshold concentrations, according to an XOR switch in the case of x_1 and a NAND switch in the case of x_2.[2] A priori this is a rather unlikely configuration to occur in real biological networks.

---

[1] Machina and Ponosov use the term "Filippov solutions in the narrow sense" [19].

[2] The regulatory logic can be inferred by writing the equations in DNF. In the case of $b_1(x) = s^+(x_1, \theta_1) + s^+(x_2, \theta_2) - 2s^+(x_1, \theta_1) \, s^+(x_2, \theta_2)$ this yields $s^+(x_1, \theta_1) \, s^-(x_2, \theta_2) + s^-(x_1, \theta_1) \, s^+(x_2, \theta_2)$, which corresponds to a Boolean XOR function. The function $b_2(x) = 1 - s^+(x_1, \theta_1) \, s^+(x_2, \theta_2)$ is the algebraic equivalent of a Boolean NAND, that is, $s^-(x_1, \theta_1) \, s^-(x_2, \theta_2) + s^+(x_1, \theta_1) \, s^-(x_2, \theta_2) + s^-(x_1, \theta_1) \, s^+(x_2, \theta_2)$.
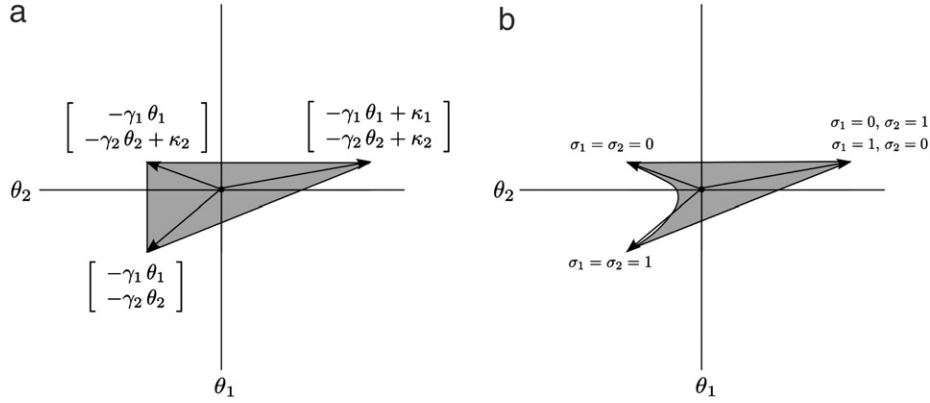
Fig. 2. The F- and AP-extensions of the PWL model (18) are different at $x = (\theta_1, \theta_2)^T$, the intersection point of the thresholds. (a) $\mathbf{F}(x)$, defined by (19), is the smallest closed convex set containing the vector fields of the four neighboring regions of $x = (\theta_1, \theta_2)^T$, evaluated at the intersection point. (b) $\mathbf{G}(x)$ is obtained by varying the parameters σ_1, σ_2 over the interval $[0, 1]$, as defined in (20). It includes the vector fields in the neighboring regions of $x = (\theta_1, \theta_2)^T$, which are obtained when σ_1, σ_2 take their extreme values 0 or 1. The plots are obtained for $\kappa_1 > \gamma_1 \theta_1$ and $\kappa_2 > \gamma_2 \theta_2$.

The following result shows that under Assumptions 2 and 4, which are usually not restrictive in practice, the different solution concepts proposed in the previous section coincide. Let us formulate a simple result on the image of a multi-affine function.

Lemma 11. *Let $g : \mathbb{R}^p \to \mathbb{R}$ be a multi-affine function. Let us denote a p-dimensional box H of $\mathbb{R}^p$ by $H = \times_{j=1}^p [l_j, u_j]$, with $l_j \leq u_j$. Then the set $g(H)$ is a closed interval in $\mathbb{R}$.*

Proof. A scalar multi-affine function $g : \mathbb{R}^p \to \mathbb{R}$ can be written as

$$g(x) = \sum_{i_1, \ldots, i_N \in \{0,1\}} c_{i_1, \ldots, i_N} \prod_{j=1}^N x_j^{i_j}. \tag{21}$$

Using the convention that $[l_j, u_j]^0 = \{1\}$ and $[l_j, u_j]^1 = [l_j, u_j]$, the set $\left\{ \prod_{j=1}^N x_j^{i_j} \mid x \in H \right\} = \prod_{j=1}^N [l_j, u_j]^{i_j}$ is a closed interval that can be denoted by $I_{i_1, \ldots, i_N}$. Hence, $g(H)$ can be expressed as a sum of closed interval:

$$g(H) = \sum_{i_1, \ldots, i_N \in \{0,1\}} c_{i_1, \ldots, i_N} I_{i_1, \ldots, i_N}, \tag{22}$$

and therefore, is a closed interval in $\mathbb{R}$. □

Proposition 12. *Under Assumptions 2 and 4, $\mathbf{F}(x) = \mathbf{G}(x)$ for all $x \in \Omega$.*

Proof. We will prove the proposition by showing that $\mathbf{G}(x) = \overline{co}(\mathbf{G}(x))$, so that the equality of $\mathbf{F}(x)$ and $\mathbf{G}(x)$ directly follows from Proposition 10.

For a given vector $x \in \mathbb{R}^n$, the vector $\sigma \in [0, 1]^p \subset \mathbb{R}^p$ belongs to the p-dimensional box H defined by

$$H = \times_{j=1}^n \times_{k=1}^{p_j} [l_j^k, u_j^k] \tag{23}$$

with $l_j^k = u_j^k = 0$ if $x_j^k < \theta_j^k$, $l_j^k = u_j^k = 1$ if $x_j^k > \theta_j^k$ and $l_j^k = 0, u_j^k = 1$ if $x_j^k = \theta_j^k$. Following Definition 8, $\mathbf{G}_i(x)$ can be written in terms of $g_i(\sigma)$ as

$$\mathbf{G}_i(x) = \{\gamma x_i\} + \{g_i(\sigma) \mid \sigma \in H\}. \tag{24}$$

Since $\{g_i(\sigma) \mid \sigma \in H\}$ is the image of a box by a multi-affine function, from Lemma 11, we conclude that it is a closed interval. From (24), we deduce that $\mathbf{G}_i(x)$ is a closed interval.

Due to Assumption 4, the vector $\sigma \in [0, 1]^p$ can be partitioned into n nonoverlapping subsets $\rho_i, i \in \{1, \ldots, n\}$ and $g_i(\sigma) = g_i(\rho_i)$. As a consequence, all $g_i(\rho_i)$ and therefore $\mathbf{G}_i(x)$ can be independently varied, $i \in \{1, \ldots, n\}$. In other words, $\mathbf{G}(x)$ can be

written as $\mathbf{G}_1(x) \times \cdots \times \mathbf{G}_n(x)$ and is a closed hyperrectangle. As a consequence, $\mathbf{G}(x)$ is a closed convex set and $\mathbf{G}(x) = \overline{co}(\mathbf{G}(x)) = \mathbf{F}(x)$ using Proposition 10. □

The PWL model of Fig. 1 satisfies Assumptions 2 and 4, so that for this example the two Filippov extensions are equivalent. This can be illustrated for the point $x = (\theta_1^1, \theta_2^1)^T$, on the intersection of the lower thresholds of x_1 and x_2. According to Definition 5, we have

$$\mathbf{F}(x) = \begin{bmatrix} -\gamma_1 x_1 \\ -\gamma_2 x_2 \end{bmatrix} + \overline{co} \left\{ \begin{bmatrix} 0 \\ 0 \end{bmatrix}, \begin{bmatrix} \kappa_1 \\ 0 \end{bmatrix}, \begin{bmatrix} 0 \\ \kappa_2 \end{bmatrix}, \begin{bmatrix} \kappa_1 \\ \kappa_2 \end{bmatrix} \right\}. \tag{25}$$

Fig. 3(a) shows the convex combination of the vector fields in the four regions having $(\theta_1^1, \theta_2^1)^T$ in their boundary, evaluated at this point and assuming that $\kappa_1 > \gamma_1 \theta_1^2$ and $\kappa_2 > \gamma_2 \theta_2^2$. The AP-extension of the PWL model (4), according to Definition 8, is defined as follows:

$$\mathbf{G}(x) = \left\{ \begin{bmatrix} -\gamma_1 x_1 + \kappa_1 \sigma_2^1 \\ -\gamma_2 x_2 + \kappa_2 \sigma_1^1 \end{bmatrix} \middle| \sigma_1^1, \sigma_2^1 \in [0, 1] \right\}. \tag{26}$$

Fig. 3(b) shows that $\mathbf{G}(x) = \mathbf{F}(x)$, as expected from Proposition 10.

The F and G-extensions in the latter example are rectangular. More generally, this can be shown to be the case, by making explicit an intermediate result in the proof of Proposition 12.

Corollary 13. *Under Assumptions 2 and 4, $\mathbf{F}(x)$ and $\mathbf{G}(x)$ are hyperrectangular sets.*

The qualitative analysis developed in [22,33], and implemented in the computer tool GNA, exploits the mathematical properties of hyperrectangular overapproximations of the convex sets used in the classical Filippov approach. In particular, they facilitate the construction of discrete abstractions of the continuous dynamics, in the form of state transition graphs, in the absence of precise quantitative information on the model parameters [12,22]. The above corollary shows that under reasonable and verifiable modeling assumptions, the results obtained are the same as those obtained with the F- and AP-extensions of Definitions 5 and 8, respectively. In other words, under the assumptions of Proposition 12, the hyperrectangular sets are not overapproximations but exact.

While a qualitative analysis is appropriate for certain problems, the absence of precise quantitative predictions is not desirable in others, such as the analysis of a limit cycle [9] or the design of a controller for a synthetic network [11]. The quantitative study of PWL models of gene regulatory networks is hindered by the fact that, as of now, no general and efficient tool for
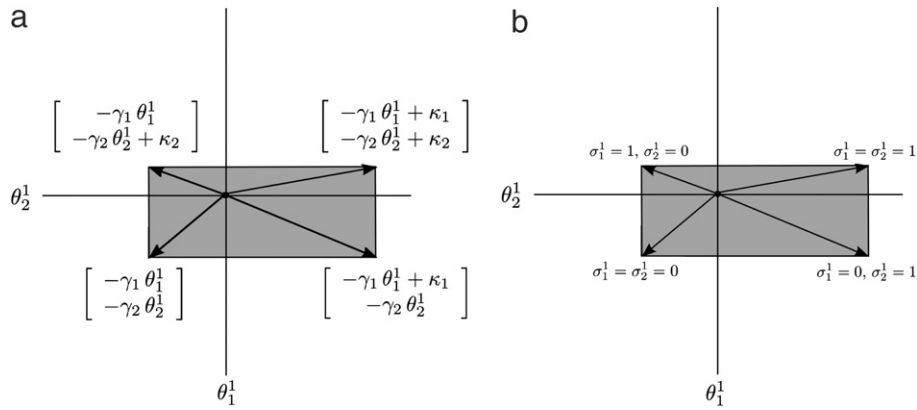
Fig. 3. The F- and AP-extensions of the PWL model (4) are identical at the threshold intersection $x = (\theta_1^1, \theta_2^1)^T$. (a) $\mathbf{F}(x)$, defined by (25), is the smallest closed convex set containing the vector fields of the four neighboring regions of $x = (\theta_1^1, \theta_2^1)^T$, evaluated at the intersection point. (b) $\mathbf{G}(x)$ is obtained by varying the parameters σ_1^1, σ_2^1 over the interval [0, 1], as defined in (26). The plots are obtained for $\kappa_1 > \gamma_1 \theta_1^2$ and $\kappa_2 > \gamma_2 \theta_2^2$.

the numerical simulation of Filippov extensions is available. In the remainder of this paper we show how tools developed for the simulation of nonsmooth mechanical, electrical and control systems [26,29,44,45] can be adapted for this purpose.

4. Numerical methods for AP-extensions of PWL systems

In this section, we propose numerical methods for performing the time-integration of the AP-extension in Definition 8 and for computing its equilibrium points. General results of convergence (and existence) of solutions are beyond the scope of this paper, but we prove under the assumption that $g(\cdot)$ is continuous (satisfied under Assumption 2) that the discrete *one-step problem* is always solvable. In practice, we can therefore always numerically compute a solution of the time-discretized problem. In other words, this enables the computation of a selection in the set-valued AP-extension $\mathbf{G}(\cdot)$ for the time-discrete system.

4.1. Reformulation of PWL models as mixed complementarity systems (MCS)

The main features of the proposed numerical time-integration method are the following:

1. A reformulation of the set-valued relation

$$\sigma \in S^+(x, \theta) \tag{27}$$

in terms of well-known concepts from Convex Analysis and Optimization Theory (inclusion into normal cones, Complementarity Problems (CP) and finite-dimensional Variational Inequalities (VI), see [46,47]). One of the interests for introducing such concepts is the extensive amount of work that has been done for their mathematical analysis and their numerical treatment (see [46,48] for an overview).
2. An implicit event-capturing time-stepping scheme, mainly based on the backward Euler scheme, which allows to deal with the switch-like behavior of the flow without resorting to an accurate detection of events. Furthermore, when a sliding motion occurs, such a scheme avoids the "chattering" effect when an attractive surface is reached [45].
3. The use of efficient numerical solvers for the *one-step problem* resulting from the time-discretization of the CP/VI formulation. At each time-step, we have to solve a CP (or equivalently a VI) for which numerous efficient solvers exist [46,49–52]. Efficient enumerative algorithms may also be used to list all possible solutions. When we are concerned with following a single solution trajectory, standard solvers for CP/VI succeed in doing this in an efficient way.

Let us start with the equivalent formulation of (27) as an inclusion in the normal cone to the interval [0, 1]. We recall the definition of the normal cone to a convex set C at a point $\sigma \in C$:

$$N_C(\sigma) = \{x \mid x^T(\sigma' - \sigma) \le 0 \text{ for all } \sigma' \in C\}. \tag{28}$$

By noting that

$$N_{[0,1]}(\sigma) = \begin{cases} \mathbb{R}_- & \sigma = 0 \\ 0, & \sigma \in [0, 1] \\ \mathbb{R}_+ & \sigma = 1, \end{cases} \tag{29}$$

the relation

$$\sigma \in S^+(x, \theta) \tag{30}$$

can equivalently be reformulated as the following inclusion

$$(x - \theta) \in N_{[0,1]}(\sigma). \tag{31}$$

In turn, the relation (31) is equivalent to the complementarity conditions

$$\begin{cases} 0 \le 1 - \sigma \perp (x - \theta)^+ \ge 0 \\ 0 \le \sigma \perp (x - \theta)^- \ge 0, \end{cases} \tag{32}$$

where the symbol $x \perp y$ means $x^T y = 0$ and y^+, y^- stand for the positive and negative parts of y, respectively. Finally, an equivalent formulation of (31) is given by the following VI : find $\sigma \in [0, 1]$ such that

$$(\theta - x)^T(\sigma - \sigma') \ge 0 \quad \text{for all } \sigma' \in [0, 1]. \tag{33}$$

Let us define the notion of modes for the solution of the inclusion (31), or equivalently for the CP/VI formulations. Each solution is associated to a triplet of index sets

$$\begin{aligned} \mathfrak{L}_+ &= \{(j, k) \in \{1 \dots n\} \times \{1 \dots p_j\} \mid \sigma_j^k = 1, x_j - \theta_j^k \ge 0\} \\ \mathfrak{L}_0 &= \{(j, k) \in \{1 \dots n\} \times \{1 \dots p_j\} \mid \sigma_j^k \in (-1, 1), \\ & \quad x_j - \theta_j^k = 0\} \\ \mathfrak{L}_- &= \{(j, k) \in \{1 \dots n\} \times \{1 \dots p_j\} \mid \sigma_j^k = -1, x_j - \theta_j^k \le 0\}, \end{aligned} \tag{34}$$

such that $card(\mathfrak{L}_+ \cup \mathfrak{L}_- \cup \mathfrak{L}_0) = p$. A mode $M_\alpha \subset \Omega \times \mathbb{R}^p, \alpha \in \{1, \dots, 3^p\}$ is defined by the set of couples (x, σ) such that the triplet of index-sets is equal to a given constant triplet of index sets. Since, in $\mathbb{N}^p$, there are 3^p possibilities to choose these triplets, the total number of modes is 3^p.

Let us now define the affine function $y : \mathbb{R}^n \to \mathbb{R}^p$ such that

$$
y(x) = Cx - \theta = \begin{bmatrix} x_1 - \theta_1^1 \\ \vdots \\ x_1 - \theta_1^{p_1} \\ \vdots \\ x_n - \theta_1^n \\ \vdots \\ x_n - \theta_1^{p_n} \end{bmatrix}^T \in \mathbb{R}^p, \tag{35}
$$

where $C \in \mathbb{R}^{p \times n}$, with $C_{ij} \in \{0, 1\}$, and $\theta = [\theta_1^1, \ldots, \theta_1^{p_1}, \ldots, \theta_n^1, \ldots, \theta_n^{p_n}]^T$. Using the formulation (31) and the definition of $y(\cdot)$, the AP-extension of the PWL system (17) in Definition 8 can be written compactly as

$$
\begin{cases} \dot{x} = -\mathrm{diag}(\gamma)x + g(\sigma) \\ y(x) = Cx - \theta \in \mathrm{N}_{[0,1]^p}(\sigma) \end{cases} \tag{36}
$$

where $\mathrm{diag}(\gamma) \in \mathbb{R}^{n \times n}$ is the diagonal matrix composed of γ_i, $i \in \{1 \ldots n\}$.

When rewritten in the form (36), the system is a Mixed Complementarity System (MCS). MCSs are an extension of Linear Complementarity Systems (LCS) [27] to the nonlinear case with nontrivial bounds on σ. LCS and MCS enter in the more general framework of Differential Variational Inequalities [28] where the solution set of a variational inequality comes into play in the right-hand side of an ordinary differential equation. For more details on complementarity systems and their relations with other types of nonsmooth dynamical systems, we refer to [26,53,54].

Remark 14 (*Equilibrium (Stationary) Points*). Finding equilibrium points of the AP-extension of PWL systems is equivalent to solving the following MCP

$$
\begin{cases} 0 = -\mathrm{diag}(\gamma)x + g(\sigma) \\ y(x) = Cx - \theta \in \mathrm{N}_{[0,1]^p}(\sigma) \end{cases} \tag{37}
$$

or more compactly

$$
C \, \mathrm{diag}(1/\gamma)g(\sigma) - \theta \in \mathrm{N}_{[0,1]^p}(\sigma). \tag{38}
$$

Using the fact that $\sigma \mapsto C \, \mathrm{diag}(1/\gamma)g(\sigma) - \theta$ is a continuous function and $[0, 1]^p$ is a compact convex set of $\mathbb{R}^p$, the VI/CP (38) has a nonempty compact set of solutions (direct application of Corollary 2.2.5 in [46, page 148]).

Equilibrium points can then be computed by solving the following problem

$$
\begin{cases} C \, \mathrm{diag}(1/\gamma)g(\sigma) - \theta \in \mathrm{N}_{[0,1]^p}(\sigma) \\ x = \mathrm{diag}(1/\gamma)g(\sigma) \\ x \in \mathbb{R}_+^n. \end{cases} \tag{39}
$$

4.2. The general time-discretization framework

Numerical time-integration of an MCS (36) can be performed by two main families of solvers.

The first one, often called event-detecting (or event-driven) time-stepping schemes, performs an accurate location of the time of events. An event corresponds to a change of mode of solutions as defined in the previous section. Between two events, any algorithm for Differential Algebraic Equations (DAEs) can be used for the time integration of the smooth dynamics. In addition to the problem of the drift of constraints when the trajectory is sliding, which can render the detection of events difficult, the main drawback of event-detecting schemes is the inability to deal with infinite

accumulations of events in finite time (also termed as Zeno-phenomena). In the context of ordinary differential equations with a discontinuous right-hand side, an event-driven scheme for a class of piecewise-smooth systems reformulated as complementarity systems is rigorously described in [55]. For an overview of event-driven schemes for nonsmooth systems, we refer to [26, Chapter 7].

The second family of schemes is the class of the event-capturing time-stepping schemes. In this case, no accurate detection of events is performed and the events may occur within the time-step. Although these methods are of low order, they are robust, stable and enjoy some convergence results under specified assumptions (see the survey paper [56] in the context of general differential inclusions). Moreover, they are able to deal with an infinite number of events in finite time, which is common in practice (see the example in Section 6.2).

For our specific class of inclusions, we are interested in developing a dedicated event-capturing time-stepping scheme which takes benefits from the special structure of the complementarity systems. As we said before, for such systems, the discretization results at each time-step in a CP/VI for which there exists a large amount of efficient algorithms. Therefore, computing a selection of the right-hand side set-valued map of our time-discretization differential inclusion can be done in a very efficient way. For general studies and a survey on time-stepping schemes for complementarity systems, we refer to [28,57–59] and [26, Chapter 9].

Let us now expose the proposed time discretization of (36) over a time-interval $[t_k, t_{k+1}]$ of length h:

$$
\begin{cases} x_{k+1} = x_k - h \, \mathrm{diag}(\gamma)x_{k+\tau} + h \, g(\sigma_{k+1}) \\ y_{k+1} = Cx_{k+1} - \theta \\ y_{k+1} \in \mathrm{N}_{[0,1]^p}(\sigma_{k+1}), \end{cases} \tag{40}
$$

with the initial condition $x_0 = x(t_0)$. The notation $x_{k+\tau}$ means $\tau x_{k+1} + (1 - \tau)x_k$ for $\tau \in [0, 1]$. The problem (40) is called the *one-step problem* that we have to solve on each interval. Let us define the vector

$$
z_{k+1} = \begin{bmatrix} x_{k+1} \\ \sigma_{k+1} \end{bmatrix} \in \mathbb{R}^{n+p}, \tag{41}
$$

and the function $F : \mathbb{R}^{n+p} \to \mathbb{R}^{n+p}$ as

$$
F(z_{k+1}) = \begin{bmatrix} x_{k+1} - x_k + h \, \mathrm{diag}(\gamma)x_{k+\tau} - h \, g(\sigma_{k+1}) \\ \theta - Cx_{k+1} \end{bmatrix}. \tag{42}
$$

Then the problem (40) is equivalent to the following inclusion

$$
-F(z_{k+1}) \in \mathrm{N}_{\mathbb{R}^n \times [0,1]^p}(z_{k+1}). \tag{43}
$$

Proposition 15. *Let $F : \mathbb{R}^{n+p} \to \mathbb{R}^{n+p}$ be the function defined in (42). Under Assumption 2, the problem of finding $z \in \mathbb{R}^n \times [0, 1]^p$ such that*

$$
-F(z) \in \mathrm{N}_{\mathbb{R}^n \times [0,1]^p}(z) \tag{44}
$$

has a nonempty and compact solution set.

Proof. The proof is based on the application of Corollary 2.2.5 in [46, page 148] which states that the VI

$$
y(\sigma)^T(\sigma - \sigma') \geq 0, \quad \text{for all } \sigma' \in K \subset \mathbb{R}^p, \tag{45}
$$

has a solution if K is compact convex, and $y : K \to \mathbb{R}^p$ is continuous. The inclusion (43) can be restated as

$$
\begin{cases} x - x_k + h \, \mathrm{diag}(\gamma)(\tau x + (1 - \tau)x_k) - h \, g(\sigma_{k+1}) = 0 \\ Cx - \theta \in \mathrm{N}_{[0,1]^p}(\sigma). \end{cases} \tag{46}
$$

Since the matrix $I_n + h\tau \, \mathrm{diag}(\gamma)$ is regular, we can solve the first equation for x. This yields the following definition of $y(\cdot)$:

$$y(\sigma) = Cx - \theta = C \, \mathrm{diag}(1/(1 + h\tau\gamma))\Big[(I_n - h(1 - \tau)$$
$$\times \mathrm{diag}(\gamma))x_k + h \, g(\sigma)\Big] - \theta, \tag{47}$$

where $\mathrm{diag}(1/(1 + h\tau\gamma))$ is the diagonal matrix made of the components $1/(1 + h\tau\gamma_i), i \in \{1 \ldots n\}$. The inclusion in (46) becomes

$$y(\sigma) \in \mathrm{N}_{[0, 1]^p}(\sigma) \tag{48}$$

and then is equivalent to (45). Since g is multi-affine, y is continuous. Choose $K = [0, 1]^p$ which is compact convex. Then, the VI (45) has a nonempty and compact solution set for σ. The relation

$$x = \mathrm{diag}(1/(1 + h\tau\gamma)) \left[(I_n - h(1 - \tau) \, \mathrm{diag}(\gamma))x_k + h \, g(\sigma) \right] \tag{49}$$

allows to build a nonempty and compact set of solutions for $z = [x \; \sigma]^T$ for (44). $\quad\square$

Remark 16. The following observations can be made:

- Proposition 15 is crucial for the success of the numerical scheme which is proposed in this paper. It states that we can always find a solution of the discrete problem. It remains to be discussed how to effectively compute one of these solutions.
- Only Assumption 2 is necessary to prove the result. It could even be relaxed to continuous functions $g(\cdot)$ instead of multi-affine.
- To avoid any misunderstanding, we have said nothing about the convergence of the scheme and we cannot straightforwardly extrapolate Proposition 15 for an existence result in continuous time. As explained above, F-extensions of PWL systems ensure the existence of solutions. The AP-extension in general does not guarantee such a result.

At each step, we have to solve the so-called *one-step* problem which has been proved to possess solutions. In the sequel, we say a few words on the solution procedures in practice. To this end, let us now introduce a fairly standard problem in Mathematical Programming, which is equivalent to the problem (40).

Definition 17 (*Mixed Complementarity Problem (MCP) [51]*)**.** Given a function $F : \mathbb{R}^{n+p} \to \mathbb{R}^{n+p}$ and lower and upper bounds $l, u \in \mathbb{R}^{n+p} \cup \{-\infty, +\infty\}$, the Mixed Complementarity Problem (MCP) is to find $z \in \mathbb{R}^{n+p}$ and $w, v \in \mathbb{R}_+^{n+p}$ such that

$$\begin{cases} F(z) = w - v \\ l \le z \le u \\ (u - z)^T v = 0 \\ (z - l)^T w = 0. \end{cases} \tag{50}$$

By choosing $l \in \{-\infty\}^n \times 0^p$ and $u \in \{+\infty\}^n \times 1^p$, solving the inclusion (43) is equivalent to solve an MCP for z_{k+1} where the vectors $w_{k+1}, v_{k+1} \in \mathbb{R}^{n+p}$ are of the form

$$(w_{k+1})_i = \begin{cases} 0, & 1 \le i \le n \\ (y_{k+1}^-)_{i-n}, & n \le i \le n + m, \end{cases}$$

$$(v_{k+1})_i = \begin{cases} 0, & 1 \le i \le n \\ (y_{k+1}^+)_{i-n}, & n \le i \le n + m. \end{cases} \tag{51}$$

Numerical algorithms for solving such problems benefit from a long experience (see [49,51] for the PATH solver and [50] for a comprehensive comparison of algorithms).

4.3. An enumerative procedure based on the Newton–Josephy approach

In most of the applications, the numerical algorithms cited in the previous section are sufficient for computing a solution of the one-step problem. Nevertheless, it can be interesting to be able to enumerate the solutions when they are multiple and isolated. To this end, we can benefit from the fact that $y(\cdot)$ is a linear function of its arguments and $g(\cdot)$ is a multi-affine application for easily applying a Newton-like method. For solving the one-step problem (43) in its MCP formulation, the Newton–Josephy method [60,61] is used which consists in a linearization of the first line of the time-discretization (40). Then, the MCP is solved by a sequential Mixed Linear Complementarity Problem (MCLP) method using a dedicated enumerative solver for MLCP.

Let us introduce the following nonlinear residue

$$\mathcal{R}(x, \sigma) = (I_n + \tau h \, \mathrm{diag}(\gamma))x$$
$$- (I_n - h(1 - \tau) \, \mathrm{diag}(\gamma))x_k - h \, g(\sigma). \tag{52}$$

The solutions x_{k+1} and σ_{k+1} of (43) satisfy $\mathcal{R}(x_{k+1}, \sigma_{k+1}) = 0$. The solutions of the nonlinear system (52) are sought as the limit of the sequence $\{x^\nu, \sigma^\nu\}_{\nu \in \mathbb{N}}$ verifying

$$\begin{cases} \mathcal{R}_L(x^{\nu+1}, \sigma^{\nu+1}) = 0 \\ x^0 = x_k, \sigma^0 = \sigma_k, \end{cases}$$

where the Newton linearization of $\mathcal{R}$ is given by

$$\mathcal{R}_L(x^{\nu+1}, \sigma^{\nu+1}) = \mathcal{R}(x^\nu, \sigma^\nu) + \nabla_x \mathcal{R}(x^\nu, \sigma^\nu)(x^{\nu+1} - x^\nu)$$
$$+ \nabla_\sigma \mathcal{R}(x^\nu, \sigma^\nu)(\sigma^{\nu+1} - \sigma^\nu).$$

Let us introduce the so-called iteration matrices

$$\begin{cases} M = \nabla_x \mathcal{R}(x, \sigma) = I_n + h\tau \, \mathrm{diag}(\gamma) \\ B(\sigma) = \nabla_\sigma \mathcal{R}(x, \sigma) = \nabla_\sigma g(\sigma). \end{cases}$$

At each time-step k, we have to solve the following linearized problem

$$x^{\nu+1} = M^{-1} \Big[(I_n - h(1 - \tau) \, \mathrm{diag}(\gamma)) x_k$$
$$+ hg(\sigma^\nu) + hB(\sigma^\nu)(\sigma^{\nu+1} - \sigma^\alpha) \Big]. \tag{53}$$

Inserting into (53) the definition of $y(\cdot)$ given by (35), we get the following linear relation between $y^{\nu+1}$ and $\sigma^{\nu+1}$

$$y^{\nu+1} = CM^{-1} \Big[(I_n - h(1 - \tau) \, \mathrm{diag}(\gamma)) x_k$$
$$+ hg(\sigma^\nu) + hB(\sigma^\nu)(\sigma^{\nu+1} - \sigma^\nu) \Big] - \theta.$$

To summarize, the problem to be solved at each Newton iteration is

$$\begin{cases} y^{\nu+1} = W^{\nu+1}\sigma^{\nu+1} + q^{\nu+1} \\ y^{\nu+1} \in \mathrm{N}_{[0, 1]^p}(\sigma^{\nu+1}), \end{cases} \tag{54}$$

where $W \in \mathbb{R}^{p \times p}$ and $q \in \mathbb{R}^p$ are defined as

$$W^{\nu+1} = h \, C \, M^{-1} B(\sigma^\nu)$$

$$q^{\nu+1} = CM^{-1} \Big[(I_n - h(1 - \tau) \, \mathrm{diag}(\gamma))x_k + hg(\sigma^\nu)$$
$$+ hB(\sigma^\nu)\sigma^\nu \Big] - \theta.$$

The problem (54) is an MLCP which can be solved under suitable assumptions by many linear complementarity solvers such as pivoting techniques, interior point techniques and splitting/projection strategies [62]. Among these techniques, some efficient enumerative solvers can also be used (see for instance [63–65]), if we are interested in enumerating several solutions corresponding to various modes of the switching functions. This approach has therefore an interest from the qualitative point of view since it allows to outline multiple solutions. More precisely, we

solve for each mode M_α a (possibly indefinite) linear system. If there are solutions existing in M_α, we can give an instance of such a solution. That is, in the numerical time integration process, we can choose to follow one particular solution corresponding to the mode. This feature will be illustrated in the oscillator example of Section 6.2.

4.4. Software aspects

The simulation platform Siconos[3] developed at INRIA [26,44,66] implements the numerical methods for AP extensions of PWL models described in the previous section. The Siconos platform is an open-source software for the modeling, simulation, analysis and control of nonsmooth dynamical systems. It has been designed and developed with a constant effort to be sufficiently general and modular to be able to deal with applications ranging over several domains, including, Mechanics, Electronics, Control, Systems Theory (see the Siconos website for examples).

In the following, we use the Siconos platform for the simulation of gene regulatory networks. In order to achieve this, the following general formulation of MCS is used

$$\begin{cases} M\dot{x} = f(x, t) + g(x, t, \lambda) \\ y = h(x, t, \lambda) \\ -y \in \mathrm{N}_{[l,u]}(\lambda) \end{cases} \tag{55}$$

where M is a non-necessarily regular matrix and $f(\cdot)$, $g(\cdot)$ and $h(\cdot)$ are assumed to be user-defined smooth functions. Without any optimization for the special case of AP-extensions given by (36), the computation time for each trajectory is between 15 ms and 1 s on a laptop computer (Apple MacBook Pro 3.60 GHz Intel Core 2 Duo). All examples presented in the next section are included in the collection of examples distributed with Siconos.

5. Illustration of the properties of the numerical methods on a two-gene regulatory network

This section is devoted to the presentation of the properties of the above numerical methods on the genetic regulatory network of two genes in Fig. 1, modeled by the two-dimensional system:

$$\begin{cases} \dot{x}_1 = -\gamma_1 x_1 + \kappa_1 s^+(x_2, \theta_2^1) s^-(x_1, \theta_1^2) \\ \dot{x}_2 = -\gamma_2 x_2 + \kappa_2 s^+(x_1, \theta_1^1) s^-(x_2, \theta_2^2), \end{cases} \tag{4}$$

with the following parameters: $\theta_1^1 = \theta_2^1 = 4, \theta_1^2 = \theta_2^2 = 8, \kappa_1 = \kappa_2 = 40, \gamma_1 = 4.5$ and $\gamma_2 = 1.5$. In particular, we detail the MCS formulation and we propose an analysis in a subset of Ω where all surfaces are attractive. We show that the proposed formulation enables one to show the uniqueness of the solution of the one-step problem and the finite-time stability of one of the equilibrium points.

5.1. MCS formulation and stability analysis

We have $card(L) = 2, n = 2$ and $p = 4$. Let $y(x) = \left[x_1 - \theta_1^1, x_1 - \theta_1^2, x_2 - \theta_2^1, x_2 - \theta_2^2\right]^T$ and $\sigma \in \mathbb{R}^4$. We also have

$$g(\sigma) = \begin{bmatrix} \kappa_1 \sigma_2^1 (1 - \sigma_1^2) \\ \kappa_2 \sigma_1^1 (1 - \sigma_2^2) \end{bmatrix},$$

$$B(\sigma) = \begin{bmatrix} 0 & -\kappa_1 \sigma_2^1 & \kappa_1 (1 - \sigma_1^2) & 0 \\ \kappa_2 (1 - \sigma_2^2) & 0 & 0 & -\kappa_2 \sigma_1^1 \end{bmatrix},$$

$$M = I_2 + h\tau \begin{bmatrix} \gamma_1 & 0 \\ 0 & \gamma_2 \end{bmatrix}, \qquad C = \begin{bmatrix} 1 & 0 \\ 1 & 0 \\ 0 & 1 \\ 0 & 1 \end{bmatrix}. \tag{56}$$

3 http://siconos.gforge.inria.fr.

There are three equilibrium points, two of which are attractive $((0, 0)$ and $(\theta_1^2, \theta_2^2))$ and a third one repulsive $((\theta_1^1, \theta_2^1))$. We focus on the equilibrium point $x_1 = \theta_1^2$ and $x_2 = \theta_2^2$ by restricting the domain of interest to $\bar{\Omega} = \Omega \cap (\theta_1^1, +\infty) \times (\theta_2^1, +\infty)$. In $\bar{\Omega}$, we have $\sigma_1^1 = 1$ since $x_1 > \theta_1^1$, and $\sigma_2^1 = 1$ since $x_2 > \theta_2^1$, so that the original system (36) can be reduced to

$$\begin{cases} \dot{x} = -\mathrm{diag}(\gamma)x + \bar{B}\bar{\sigma} + \bar{\kappa} \\ \bar{C}x - \bar{\theta} \in \mathrm{N}_{[0,1]^2}(\bar{\sigma}), \end{cases} \tag{57}$$

with

$$\bar{\sigma} = \begin{bmatrix} \sigma_1^2 \\ \sigma_2^2 \end{bmatrix}, \qquad \bar{C} = \begin{bmatrix} 1 & 0 \\ 0 & 1 \end{bmatrix}, \qquad \bar{\theta} = \begin{bmatrix} \theta_1^2 \\ \theta_2^2 \end{bmatrix},$$

$$\bar{B} = \begin{bmatrix} -\kappa_1 & 0 \\ 0 & -\kappa_2 \end{bmatrix}, \qquad \bar{\kappa} = \begin{bmatrix} \kappa_1 \\ \kappa_2 \end{bmatrix}. \tag{58}$$

The complementarity systems (or equivalently, differential variational inequalities) framework provides not only an efficient framework for simulation, but it can also help us to conclude on the stability, possibly in finite-time, of the equilibrium point (θ_1^2, θ_2^2) in $\bar{\Omega}$. On one hand, the study of the stability of PWL systems for gene regulatory networks has already been studied in [13], while on the other hand there is a huge literature dealing with the stability of Filippov systems and differential inclusions, and in particular of the finite-time stability [41]. We do not wish to give an exhaustive treatment of the stability of PWL systems by means of monotone differential inclusions, which is beyond the scope of the paper. The following result, however, gives an idea of the large range of applicability of the complementarity systems techniques.

Lemma 18. *The equilibrium point $\bar{\theta} = (\theta_1^2, \theta_2^2)^T$ is finite-time stable in $\bar{\Omega}$.*

Proof. Since $-\bar{B}$ is a symmetric definite positive matrix, we choose a symmetric positive definite matrix R as a square root of the inverse of $\bar{B}$, i.e. $R^2 = -\bar{B}^{-1}$. Following [67], let us perform the state transformation $z = R(x - \bar{\theta})$. The solution of the reduced system (57) is equivalent to the following inclusion

$$-\dot{z} \in T(z), \tag{59}$$

with the multi-valued operator T defined as

$$T(z) = R\,\mathrm{diag}(\gamma)R^{-1}z + (\mathrm{diag}(\gamma)\bar{\theta} - \bar{\kappa}) + R^{-1}S^+(R^{-1}z, 0). \tag{60}$$

Since $S^+(\cdot, 0)$ is monotone and $R = R^T$, $R^{-1}S^+(R^{-1}\cdot, 0)$ is also monotone [48, Exercise 12.4]. Since R is a diagonal matrix, we have $R\,\mathrm{diag}(\gamma)R^{-1} = \mathrm{diag}(\gamma)$ which obviously is a positive definite matrix. As a consequence, the operator $T(\cdot)$ is a strongly monotone mapping in $\bar{\Omega}$, i.e., there exists $c > 0$

$$(\lambda' - \lambda)^T(x - y) \geq c\|x - y\|^2,$$
$$\forall x, y \in \bar{\Omega}, \ \forall \lambda' \in T(x), \forall \lambda \in T(y). \tag{61}$$

Let us compute the set $T(0)$

$$T(0) = -\mathrm{diag}(\gamma)\bar{\theta} + \bar{\kappa} + \bar{B}S^+(\bar{\theta}, \bar{\theta})$$
$$= [-36, 4] \times [-12, 28]. \tag{62}$$

The existence of an equilibrium point for $x = \bar{\theta}$ is ensured by $0 \in T(0)$. Choosing a Lyapunov function $V(z) = 1/2z^2$, we have $V(0) = 0, V(z) \geq 0$ for all z and

$$\dot{V}(z) = z^T\dot{z} \quad \text{with} \ -\dot{z} \in T(z). \tag{63}$$

Since $T(\cdot)$ is strongly monotone and $0 \in T(0)$, we can conclude that $\dot{V}(z) \leq c\|z\|^2, c > 0$ and that the equilibrium point is
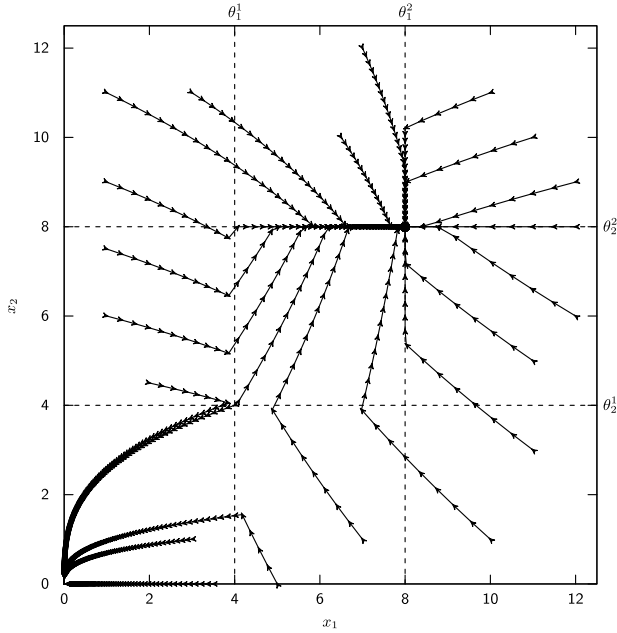
Fig. 4. Different trajectories of the two-gene regulatory network in Fig. 1 defined by (4). The different trajectories illustrate that the system has three equilibrium points (of which are two stable and one unstable).

exponentially stable. To prove the finite-time stability, we use the fact that $T(\cdot)$ is simply monotone,

$$(\lambda' - \lambda)^T(x - y) \geq 0, \quad \forall x, y \in \bar{\Omega}, \ \forall \lambda' \in T(x), \ \forall \lambda \in T(y) \quad (64)$$

in conjunction with the fact that there exists a ball of radius $r \in (0, 4)$ included in $T(0)$:

$$B_r(0) = \{z \mid \|z\| \leq r\} \subset T(0). \quad (65)$$

For $-\lambda \in T(z)$ and $-\lambda_0 \in T(0)$, we get

$$(\lambda - \lambda_0)^T z \leq 0. \quad (66)$$

Choosing $z \neq 0$ and $-\lambda_0 = -rz/\|z\| \in B_r(0) \subset T(0)$, we have

$$\lambda^T z \leq r \frac{z^T}{\|z\|} z = r\|z\|. \quad (67)$$

Since $-\lambda \in T(z)$, we get for $z \neq 0$,

$$\dot{V}(z) + r\sqrt{|V(z)|} \leq 0. \quad (68)$$

Assume for any $t_1 > t_0$ that $V(z(t_1)) > 0$. Then we can divide (68) by $\sqrt{|V(z)|}$ and perform a time integration between t_1 and t_0

$$\sqrt{|V(z(t_1))|} - \sqrt{|V(z(t_0))|} \leq -r(t_1 - t_0). \quad (69)$$

From (69), we infer that $\lim_{t_1 \to +\infty} V(z(t_1)) = -\infty$. By contradiction, we can conclude that there exists a finite time t_1 such that $V(z(t_1)) = 0$. In other words, the equilibrium $z = 0$ is reached in finite time. $\quad\square$

In the following section, we are interested in the discrete-time properties of the numerical scheme.

5.2. Properties of the numerical simulations

In Fig. 4, several trajectories of the MCS (36), which correspond to the AP-extension of (4), have been simulated with the proposed algorithm. The simulations have been carried out over the time-interval $[0, 3]$ with a time-step equal to $h = 10^{-2}$. The integration parameter τ is chosen as $\tau = 1/2$ (mid-point scheme).

Note that the equilibrium points are perfectly reproduced by the numerical simulation. Numerical simulations also reveal two sliding surfaces $\{x_1 = \theta_1^2, \theta_2^1 < x_2\}$ and $\{x_2 = \theta_2^2, \theta_1^1 < x_1\}$. We can note that the simulated trajectories perfectly slide on these surfaces without any numerical chattering. As defined in [68], numerical chattering corresponds to the oscillations (limit cycles) which are solely due to the time-discretization of (36). Avoiding numerical chattering is mainly due to the implicit character of the scheme for the inclusion part. Semi-explicit schemes of the form

$$\begin{cases} x_{k+1} = x_k - h\,\mathrm{diag}(\gamma)x_{k+\tau} + h\,g(\sigma_k) \\ y_k = Cx_k - \theta \\ y_k \in \mathrm{N}_{[0,1]^p}(\sigma_k) \end{cases} \quad (70)$$

yield numerical chattering. Although the convergence of such schemes is proven [56], this drawback prevents qualitative analysis of solutions for a finite time-step size $h > 0$. Furthermore, the fact that the matrix $-\bar{C}\bar{B}$ is definite positive in this area makes it possible to apply Lemma 3 from [45], which ensures that numerical chattering will not occur. In Fig. 5, we show the simulation of the AP-extension of the PWL systems with the explicit Euler scheme (70) for $\tau = 0$ (Fig. 5(a)–(c)) and with the proposed implicit scheme (Fig. 5(d)–(f)). With a 10 times larger time-step, the implicit scheme reaches the sliding surface and then the equilibrium without chattering. More precisely, there exists k_0, such that $x_k = \bar{\theta}$ and $(x_{k+1} - x_k)/h = 0$ for all $k > k_0$.

In the reduced domain $\bar{\Omega}$, the one-step problem can be reduced to

$$\begin{cases} x_{k+1} = x_k - h\,\mathrm{diag}(\gamma)x_{k+\tau} + h\bar{B}\bar{\sigma}_{k+1} + h\bar{\kappa} \\ \bar{C}x_{k+1} - \bar{\theta} \in \mathrm{N}_{[0,1]^2}(\bar{\sigma}_{k+1}). \end{cases} \quad (71)$$

The Jacobian matrix is then given by

$$\bar{C}\bar{B} = \begin{bmatrix} -\kappa_1 & 0 \\ 0 & -\kappa_2 \end{bmatrix}. \quad (72)$$

Since $\kappa_i > 0$, the matrix $-\bar{C}\bar{B}$ is definite positive in $\bar{\Omega}$ and we have

$$-x^T\bar{C}\bar{B}x \geq \kappa\|x\|^2 \quad (73)$$

with $\kappa = \min(\kappa_1, \kappa_2)$. This means that the VI

$$\bar{\theta} - \bar{C}\,\mathrm{diag}(1/(1 + h\tau\gamma))$$
$$\left[(I_n - h(1 - \tau)\,\mathrm{diag}(\gamma))x_k + h\bar{B}\bar{\sigma} + h\bar{\kappa}\right] \in \mathrm{N}_{[0,1]^2}(\bar{\sigma}) \quad (74)$$

is strongly monotone and has a unique solution (see [46, Theorem 2.3.3]), given by

$$(\sigma_1^2)_{k+1} = \mathrm{proj}_{[0,1]}\left(\frac{1 + h\tau\gamma_1}{h\kappa_1}\left[\theta_1^2 - \frac{1}{1 + h\gamma_1}\right.\right.$$
$$\left.\left. \times (1 - h(1 - \tau)\gamma_1 x_{1,k+1} + h\kappa_1)\right]\right)$$
$$(\sigma_2^2)_{k+1} = \mathrm{proj}_{[0,1]}\left(\frac{1 + h\tau\gamma_2}{h\kappa_2}\left[\theta_2^2 - \frac{1}{1 + h\gamma_2}\right.\right. \quad (75)$$
$$\left.\left. \times (1 - h(1 - \tau)\gamma_2 x_{2,k+1} + h\kappa_2)\right]\right).$$

To conclude this first example, the MCS formulation with an implicit time-discretization allows us to reproduce the main features of the dynamics of the PWL models of the gene regulatory network: equilibrium points, sliding surfaces, finite-time stability. In the next section, some more realistic examples are considered.
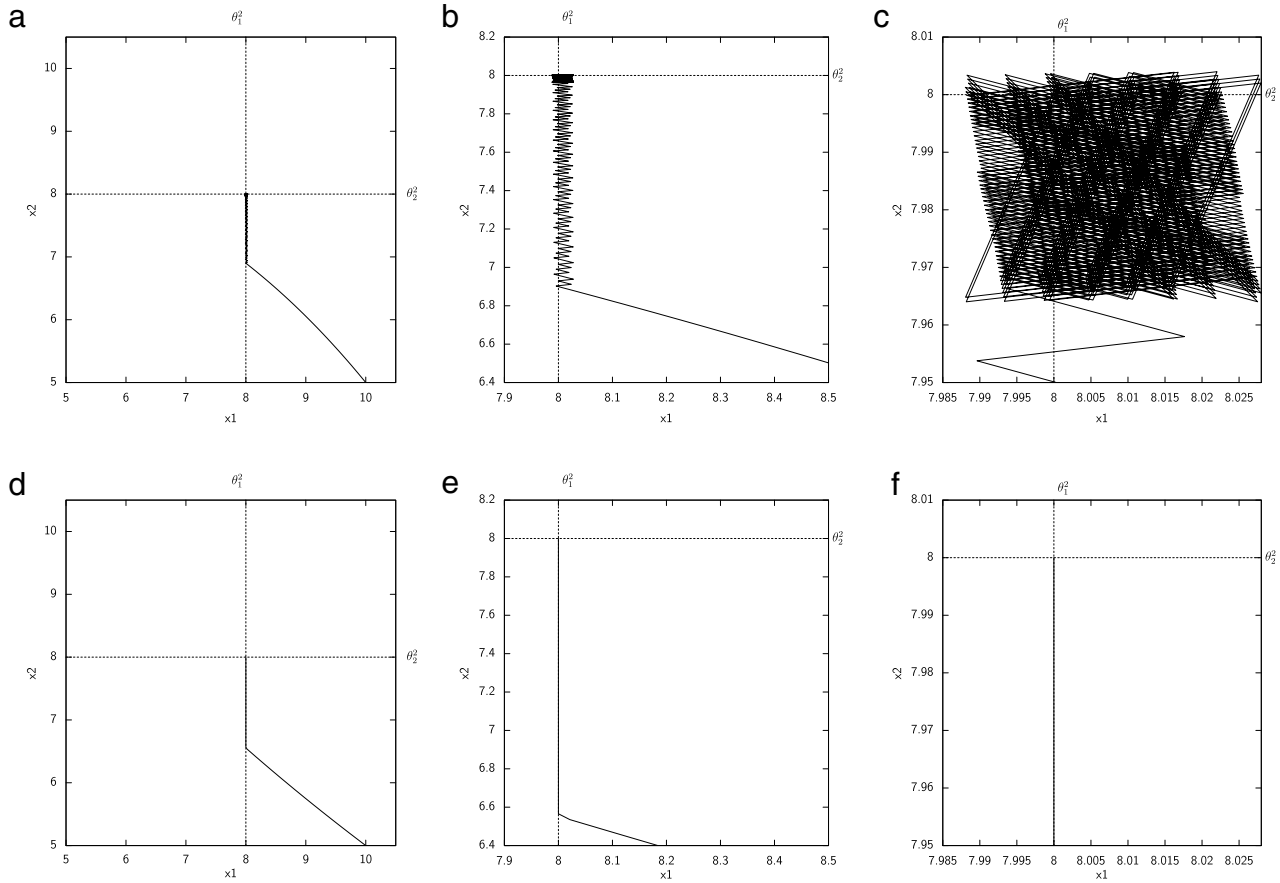
Fig. 5. Illustration of the numerical chattering effect by zooming in on the state space on the system (4) as shown in Fig. 4. The trajectories start from $x(t_0) = [10, 5]^T$. (a)–(c). Different zooms on the trajectory obtained with the explicit Euler scheme ($h = 10^{-3}$). (d)–(f). Different zooms on the trajectory obtained with the proposed implicit Euler scheme ($h = 10^{-2}$).

6. Applications in synthetic biology

In this section we apply the simulation methods developed above to the analysis of actual biological networks. We consider three examples from the field of synthetic biology [3], which all concern relatively small networks that have been designed from pre-existing, well-characterized molecular elements and implemented in the cell to perform a particular function. The first two networks have been shown able to exhibit oscillations ([30,31], see [69] for a review on synthetic oscillators). The third network is capable of a variety of dynamic behaviors and has been proposed as a benchmark for the reverse engineering of the network structure from time-course data [32]. In the three cases we transformed the network structure into PWL equations, taking inspiration from existing ODE models, and we compared the dynamic features of the networks revealed by the simulations with available experimental data.

For each of the networks described above, we determined the equilibrium points and numerically computed solutions exemplifying the dynamics of the PWL systems. The mathematical analysis of equilibrium points of PWL models (1) was based on analytical results in the literature, concerning both equilibrium points within regions separated by threshold planes ($x \notin \Theta$) and equilibrium points located on one or several threshold planes ($x \in \Theta$) [12,13,24]. While the former are always asymptotically stable in the classical sense [12], analyzing the stability of the latter requires generalized definitions adapted to the non-uniqueness of solutions of PWL systems. In particular, we used the results developed in [13] for F-extensions of PWL models (Definition 5), which provide easy-to-verify criteria for checking the stability in a number of typical cases. Notice that in the examples below, Assumptions 2 and 4 are always satisfied, which means that the F-extensions used for stability analysis and the AP-extensions used for simulation are equivalent (Proposition 12). As a consequence, the results obtained for the three example networks are valid for the different solution concepts reviewed in Section 3.

6.1. Repressilator

A repressilator is a network of several genes with a cyclic structure. Each gene codes for a transcription regulator that represses the next gene in the cycle. Elowitz and Leibler [30] have implemented a repressilator in the model bacterium *Escherichia coli*, using the genes *lacI*, *tetR*, and *cI* (Fig. 6(a)). The network can be externally controlled by adding the small inducer molecules IPTG and aTc to the growth medium, which inactivate LacI and TetR, respectively. Starting from their ODE model, we formulated a PWL model of the three-gene repressilator. The major change consists in lumping transcription and translation into a single step and replacing the sigmoidal regulation functions by step functions. The parameter values in [30] have been adapted accordingly (see Fig. 6(b)).

The PWL model of the repressilator has a single equilibrium point, in accordance with the ODE model of Elowitz and Leibler. This equilibrium point is located at the intersection of the three thresholds, that is, at $x = \theta = [\theta_1, \theta_2, \theta_3]^T$. The equilibrium point is thus also a discontinuity point of the PWL model. More precisely, the set of solutions starting from $x = \theta$ includes solutions that remain at the equilibrium point as well as solutions that leave this point at any time $t \geq 0$. For the chosen parameter values,
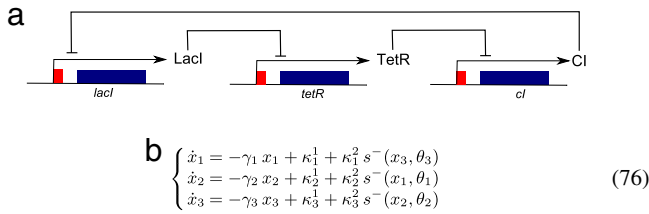
a

b
$$\begin{cases} \dot{x}_1 = -\gamma_1\, x_1 + \kappa_1^1 + \kappa_1^2\, s^-(x_3, \theta_3) \\ \dot{x}_2 = -\gamma_2\, x_2 + \kappa_2^1 + \kappa_2^2\, s^-(x_1, \theta_1) \\ \dot{x}_3 = -\gamma_3\, x_3 + \kappa_3^1 + \kappa_3^2\, s^-(x_2, \theta_2) \end{cases} \qquad (76)$$

Fig. 6. (a) Repressilator consisting of three genes [30]. The external control by the inducer molecules IPTG and aTc is not shown in the figure. (b) PWL model corresponding to the network in (a). The variables x_1, x_2, and x_3 represent the concentrations of the proteins LacI, TetR, and CI, respectively. The following parameter values have been used in the simulations: $\gamma_1 = \gamma_2 = \gamma_3 = 0.2$, $\kappa_1^1 = \kappa_2^1 = \kappa_3^1 = 4.8\ 10^{-4}$, $\kappa_1^2 = \kappa_2^2 = \kappa_3^2 = 4.8\ 10^{-1}$, and $\theta_1 = \theta_2 = \theta_3 = 1$. The time and concentration variables as well as the parameters in the model have been rescaled so as to make them dimensionless [30].

the equilibrium point is therefore unstable [13]. The numerical solver finds an infinite number of solutions starting from $x = \theta$. At each time-step, starting from the equilibrium point $x = \theta$, an enumerative MCP solver is able to give a specific solution in each mode which corresponds to staying either at the equilibrium or leaving it. This qualitative feature of the algorithm will be illustrated in detail in Section 6.2.

Fig. 7 shows an example trajectory of the model, starting from the initial state $x = 0 = [0,0,0]^T$. As can be seen, the trajectory approaches a limit cycle, again in accordance with the ODE model of Elowitz and Leibler. *In-vivo* measurements of the expression dynamics of a fluorescent reporter gene, driven by the same promoter as the gene *cI*, indicate that 40% of the analyzed cells indeed exhibit oscillations. The fact that not all cells oscillate, and that the periods and amplitudes vary between oscillating cells, can be attributed to stochastic effects that are not accounted for in deterministic ODE or PWL models [69]. The occurrence of limit cycles in repressilator models has been an active subject of research for ODE models (see [69,70] for reviews) and PWL models [11,14–16].

6.2. Synthetic oscillator with positive feedback

A second example of a synthetic oscillator network, developed by Atkinson et al. [31], is shown in Fig. 8(a). It consists of a negative feedback involving two genes, *lacI* and *glnG*: LacI inhibits the expression of *glnG*, whereas the product of the latter gene, the (phosphorylated) form of NRI (NRIp), activates *lacI*. The authors used a mutant strain which made NRI phosphorylation independent from the growth conditions, notably the cellular nitrogen status. NRIp also activates the expression of its own gene, thus giving rise to an additional positive feedback loop. While a negative feedback loop is necessary for generating oscillations, a positive feedback loop is believed to favor the robustness of the oscillations [69]. Like in the case of the repressilator, the activity of LacI can be externally controlled by varying the concentration of IPTG in the growth medium.

We constructed a PWL model of this network, given by (77) in Fig. 8(b). The model has been obtained by first formulating an ODE model using information from the paper, in the same way as for the repressilator. In particular, the model includes the design features that LacI and NRIp have antagonistic effects on *glnG* and that the binding of LacI to the promoter region shuts off the expression of the gene. Moreover, the affinity of NRIp for the promoter region upstream of *glnG* is higher than for the promoter region upstream of *lacI*. This gives rise to a lower value of the threshold associated with NRIp-activation of *glnG* than the threshold associated with NRIp-activation of *lacI* ($\theta_2^1 < \theta_2^2$). In a second step, this ODE model has been simplified by lumping the transcription and translation steps, and by replacing the sigmoidal regulation functions by step
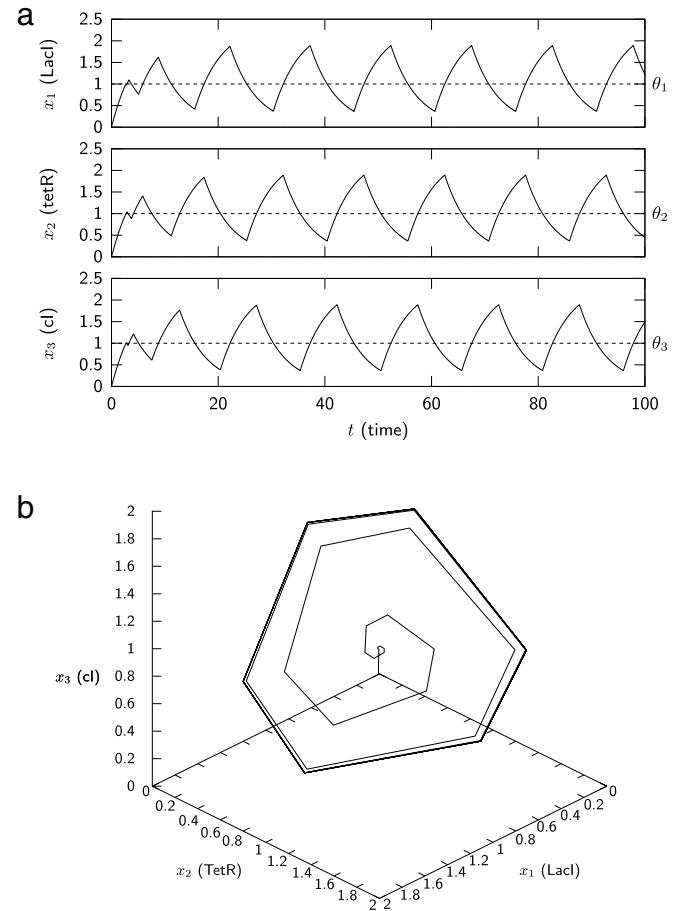

Fig. 7. Simulation of repressilator network in Fig. 6: (a) a solution starting from the initial state $x^0 = 0$ and (b) the corresponding phase-space trajectory. Notice that time is a dimensionless variable in the model [30]. Physical time can be reconstructed by multiplying the rescaled time variable in the model by $2/\ln 2$. The dashed lines represent the threshold concentrations of the variables.
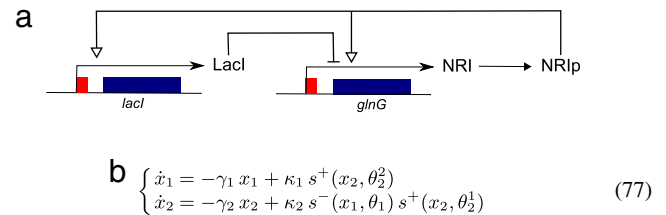

a

b
$$\begin{cases} \dot{x}_1 = -\gamma_1\, x_1 + \kappa_1\, s^+(x_2, \theta_2^2) \\ \dot{x}_2 = -\gamma_2\, x_2 + \kappa_2\, s^-(x_1, \theta_1)\, s^+(x_2, \theta_2^1) \end{cases} \qquad (77)$$

Fig. 8. (a) Oscillator with positive feedback consisting of two genes [31]. The external control by the inducer molecule IPTG is not shown in the figure. (b) PWL model corresponding to the network in (a). The variables x_1 and x_2 represent the concentrations of the proteins LacI and GlnG, respectively. The following parameter values have been used in the simulations: $\gamma_1 = \gamma_2 = 0.032$, $\kappa_1 = 0.08$, $\kappa_2 = 0.16$, and $\theta_1 = 1$, $\theta_2^1 = 1$, and $\theta_2^2 = 4$. The time and concentration variables as well as the parameters in the model have been rescaled so as to make them dimensionless, in the same way as in [30]. The dashed lines represent the threshold concentrations of the variables.

functions. The parameter values were copied from the model in [31], and where necessary completed with reasonable estimates.

The PWL model (77) has three equilibrium points, with the coordinates $(0,0)^T$, $(0, \theta_2^1)^T$, and $(\theta_1, \theta_2^2)^T$, respectively. The local dynamics around these equilibrium points are shown in Fig. 9(a). The first equilibrium point lies away from the threshold planes and is asymptotically stable [12]. The second and the third equilibrium points, on the other hand, are located on a threshold plane and on the intersection of two threshold planes, respectively. More precisely, the equilibrium point $x = (0, \theta_2^1)^T$ lies on a repulsive
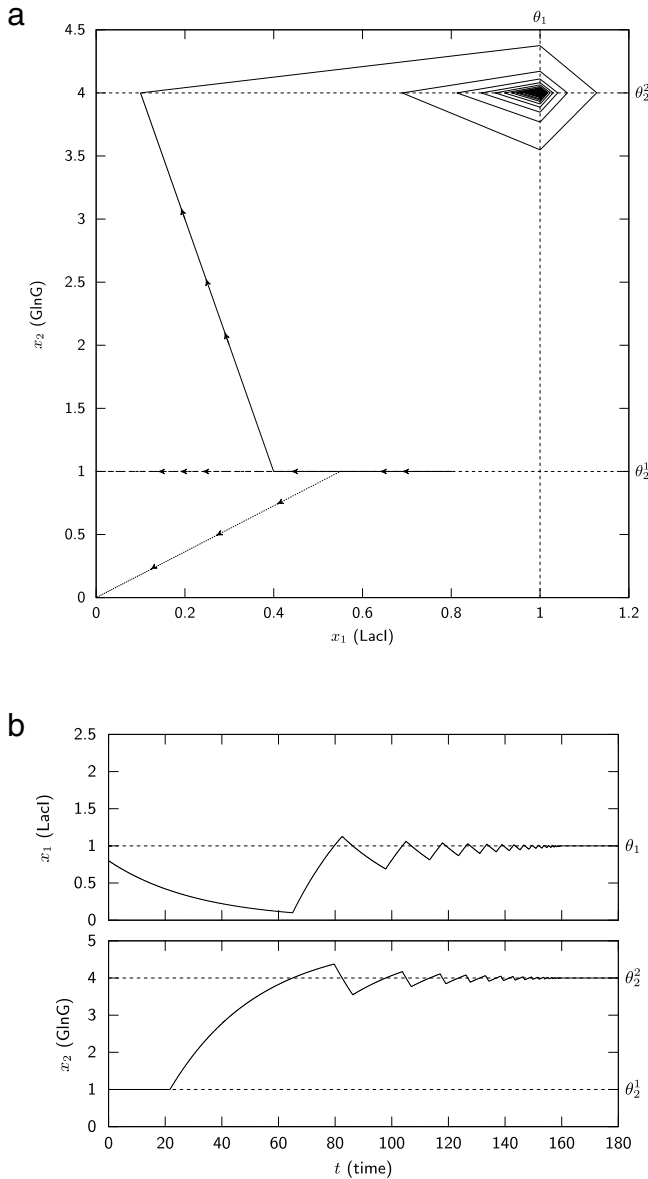
a

b

Fig. 9. Simulation of synthetic oscillator network with positive feedback in Fig. 8. (a) Trajectories corresponding to several solutions starting from the initial state $x^0 = (0.78, 1)^T$ located on the repulsive discontinuity segment separating the basins of attractions of the two asymptotically stable equilibrium points. (b) Simulation trace of the damped oscillation that corresponds to the trajectory converging towards $x = (\theta_1, \theta_2^2)^T = (1, 4)^T$. Notice that time is a dimensionless variable in the model [30]. Physical time can be reconstructed by multiplying the rescaled time variable in the model by $2/\ln 2$.

discontinuity segment, defined by $0 \leq x_1 < \theta_1$ and $x_2 = \theta_2^1$. As a consequence, it is unstable [13]. Fig. 9(a) shows that solutions starting in the neighborhood of $x = (\theta_1, \theta_2^2)^T$ converge towards this point. This illustrates that, for the chosen parameter values, this equilibrium point is asymptotically stable.

The existence of a repulsive discontinuity segment in Fig. 9 entails non-uniqueness of solutions. In fact, any solution with an initial state x^0 in the segment $0 < x_1 < \theta_1$ and $x_2 = \theta_2^1$ has an infinite number of solutions. The set of solutions includes one that, while sliding on the segment, asymptotically converges towards the equilibrium point $x = (0, \theta_2^2)^T$. The other solutions all slide for some time $\tau \geq 0$ on the segment and then escape to either the region above or below. That is, they converge towards one of the two asymptotically stable equilibrium points of the system, $x = (0, 0)^T$ or $x = (\theta_1, \theta_2^2)^T$. The discontinuity segment is the

PWL analog of a separatrix in classical ODE models. It occurs as a consequence of the positive autoregulatory interaction in the circuit of Fig. 8, corresponding to the step function $s^+(x_2, \theta_2^1)$ in the right-hand side of (77).

In Fig. 9(a), phase-space trajectories corresponding to several solutions starting from the initial state $x^0 = (0.78, 1)^T$ located on the repulsive discontinuity segment are depicted. In practice, we first performed a simulation with an enumerative solver that reveals that in the neighborhood of the repulsive segment the MLCP (54) has multiple solutions. The modes, as defined in Section 4, are recorded. Once this first simulation has been performed, the user can choose a preferred solution (encoded by one triplet of index sets) on a user-supplied part of the trajectory, by asking the numerical solver to check if a solution with the given triplet exists. For the trajectories shown in Fig. 9(a), three possible solutions have been detected in the neighborhood of the repulsive segment. A new simulation has been performed asking to prefer the triplet corresponding to the solution that slides on the segment. For the other trajectories, we changed the preferred solution when the trajectory reaches $x_1 = 0.55$ and $x_1 = 0.4$ to the triplet of solutions that yields a trajectory escaping below and above the threshold, respectively.

Atkinson et al. [31] measured the time-varying dynamics of the circuit on the population level using the chromosomal *lacZ* gene. This gene is under the control of LacI and encodes β-galactosidase, whose levels can be assayed. The authors observed damped oscillations of β-galactosidase, which correspond to the dynamics of the PWL model when the initial LacI concentration lies above its first threshold ($x_1^0 > \theta_1^1$, see Fig. 9). In order to verify that damped oscillations on the population level are not due to the desynchronization of individual cells that exhibit stable oscillations, Atkinson et al. [31] also measured gene expression in single cells, using a fluorescent reporter gene fused to a LacI-repressible promoter. The results confirm the occurrence of damped oscillations in the oscillator with positive feedback, in agreement with the population-level assay.

6.3. IRMA: a synthetic benchmark network

IRMA is a synthetic network constructed in yeast and proposed as a benchmark for modeling and identification approaches [32]. The network consists of five well-characterized genes that have been chosen so as to include different kinds of interactions, notably transcription regulation and protein–protein interactions. The structure of the IRMA network is shown in Fig. 10(a). The expression of the *CBF1* gene is positively regulated by Swi5 and negatively regulated by Ash1. *CBF1* encodes the transcription factor Cbf1 that activates expression of the *GAL4* gene. The expression of *SWI5* is activated by Gal4, but only in the absence of Gal80 or in the presence of galactose. Gal80 binds to the Gal4 activation domain, but galactose releases this inhibition of transcription. The product of *SWI5* activates the expression of three other genes in the network: *ASH1*, *CBF1*, and *GAL80*. The network contains one positive and two negative feedback loops. Consequently, for suitable parameter values IRMA might function as a synthetic oscillator [71].

Fig. 10(b) shows a PWL model of IRMA that was previously developed [36]. The regulatory functions in the model encode the interaction structure described above. Most parameter values in the PWL model were taken from the original IRMA publication. In a few cases, however, they were slightly adapted to satisfy inequality constraints between parameters that were inferred from the experimental data [36].

Using the model (78), we simulated the behavior of the network in response to two different perturbations: shifting cells from glucose to galactose medium (switch-on experiments), and from
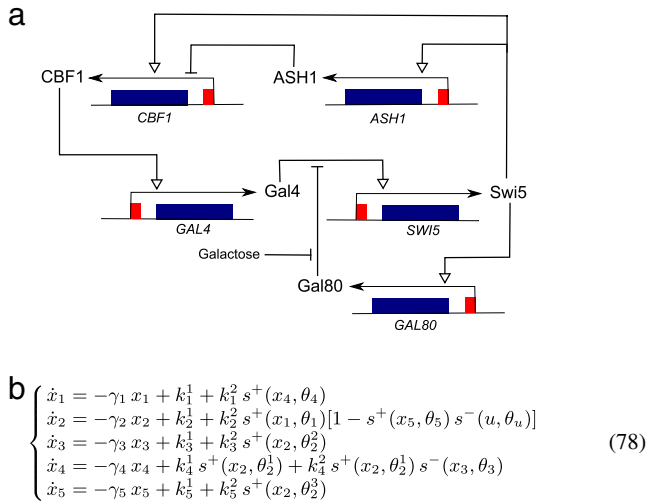
a

b
$$\begin{cases} \dot{x}_1 = -\gamma_1 x_1 + k_1^1 + k_1^2 s^+(x_4, \theta_4) \\ \dot{x}_2 = -\gamma_2 x_2 + k_2^1 + k_2^2 s^+(x_1, \theta_1)[1 - s^+(x_5, \theta_5) s^-(u, \theta_u)] \\ \dot{x}_3 = -\gamma_3 x_3 + k_3^1 + k_3^2 s^+(x_2, \theta_2^2) \\ \dot{x}_4 = -\gamma_4 x_4 + k_4^1 s^+(x_2, \theta_2^1) + k_4^2 s^+(x_2, \theta_2^1) s^-(x_3, \theta_3) \\ \dot{x}_5 = -\gamma_5 x_5 + k_5^1 + k_5^2 s^+(x_2, \theta_2^3) \end{cases} \qquad (78)$$

Fig. 10. (a) IRMA network consisting of five genes [32]. (b) PWL model corresponding to the network in (a). The variables x_1, x_2, x_3, x_4, and x_5 represent the concentrations of the proteins Gal4, Swi5, Ash1, Cbf1, and Gal80, respectively. Like in [32], these variables have arbitrary units (a.u.). In addition, the variable u represents the concentrations of external galactose, an input signal. The following parameter values have been used in the simulations: $\gamma_1 = 0.05$, $\gamma_2 = 0.04$, $\gamma_3 = 0.05$, $\gamma_4 = 0.02$, $\gamma_5 = 0.6$, $\kappa_1^1 = 1.1\,10^{-4}$, $\kappa_1^2 = 9.0\,10^{-4}$, $\kappa_2^1 = 3.0\,10^{-4}$, $\kappa_2^2 = 0.15$, $\kappa_3^1 = 6.0\,10^{-4}$, $\kappa_3^2 = 0.018$, $\kappa_4^1 = 5.0\,10^{-4}$, $\kappa_4^2 = 0.03$, $\kappa_5^1 = 7.5\,10^{-3}$, $\kappa_5^2 = 0.015$, $\theta_1 = 0.01$, $\theta_2^1 = 0.01$, $\theta_2^2 = 0.06$, $\theta_2^3 = 0.08$, $\theta_3 = 0.035$, $\theta_4 = 0.04$, and $\theta_5 = 0.01$. The units of the degradation parameters γ, κ, and θ are min^{-1}, a.u., and a.u. min^{-1}, respectively. We do not assign numerical values to u and its threshold θ_u, but rather consider separately the cases $s^+(u, \theta_u) = 0$ (switch-on) and $s^+(u, \theta_u) = 1$ (switch-off).

Fig. 11. Simulation of the response of the IRMA network in Fig. 10 in a switch-on experiment.

galactose to glucose medium (switch-off experiments). The terms switch-on (switch-off) refer to the activation (inhibition) of SWI5 expression during growth on galactose (glucose). For these two perturbations, the temporal evolution of the expression of all the genes in the network was monitored by qRT-PCR with good time resolution in [32].

In switch-off conditions, when $s^+(u, \theta_u) = 1$, the PWL system has a single asymptotically stable equilibrium point, not located on a threshold plane. At this equilibrium point all genes are expressed at their basal level $x = (\kappa_1^1/\gamma_1, \kappa_2^1/\gamma_2, \kappa_3^1/\gamma_3, 0, \kappa_5^1/\gamma_5)^T$. The measured time-series expression profiles of the five network genes in a switch-off experiment indeed show that the system evolves towards a basal state [32].

In switch-on conditions, when $s^+(u, \theta_u) = 0$, the PWL system has three equilibrium points. The first coincides with the equilibrium point in switch-off conditions. The second is an unstable equilibrium point located on the intersection of three different threshold planes ($x = (\theta_1, \theta_2^1, \kappa_3^1/\gamma_3, \theta_4, \kappa_5^1/\gamma_5)^T$). The third equilibrium point, with the coordinates $(\theta_1, \theta_2^2, \theta_3, \theta_4, \kappa_5^1/\gamma_5)^T$ is also unstable: solutions starting in its neighborhood converge towards a limit cycle.

Fig. 11 shows the simulated response of the network in a switch-on experiment, with initial conditions that are obtained by slightly perturbing the switch-off equilibrium point. As can be seen, the solutions do not contain sliding modes, in which one or more variables remain at their threshold value during a finite-time interval. The agreement of the predicted oscillations with the experimental data is unclear. Individual time-series, which were used for the parameterization of the PWL model [36], seem to exhibit oscillatory patterns. These patterns largely disappear when the data are averaged over several independent time-series (where damped oscillations are seen for Swi5 and Cbf1 only). The large error bars in the averaged experiments may hide more subtle dynamic patterns, however, and no data on the single-cell level are available.
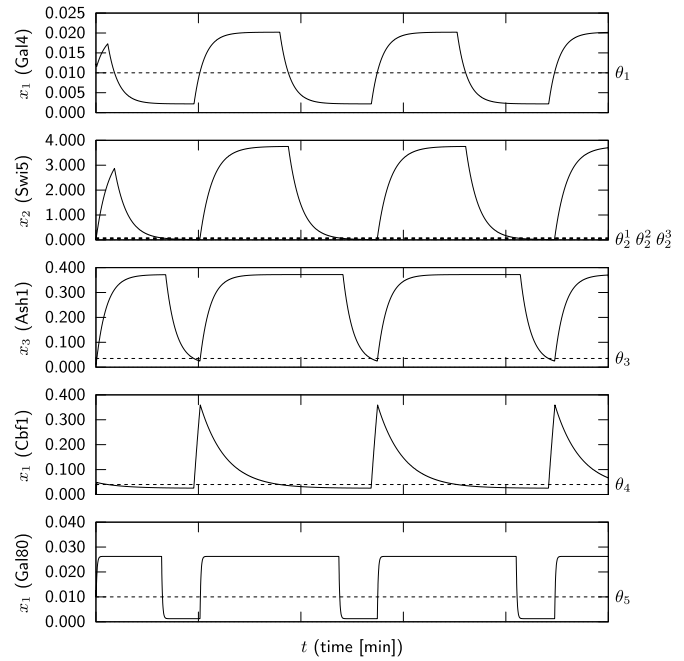
7. Discussion

We have presented a numerical method for the simulation of gene regulatory networks described by PWL models. In order to account for discontinuities in the right-hand side of the differential equations, PWL models have to be extended to differential inclusions which cannot be handled by classical ODE solvers. We show that by reformulating one such extension, the AP-extension, as a mixed complementarity system (MCS), numerical methods developed for the time-integration of nonsmooth dynamical systems are directly applicable. An extensive amount of work on the mathematical and numerical analysis of complementarity systems has been done, which provides a solid theoretical basis for the proposed method. Moreover, powerful and widely-used numerical tools for complementarity systems are available, like the SICONOS platform used here.

We have shown that under assumptions that are not restrictive in practice, the AP-extensions are equivalent with other proposed extensions of PWL models, notably classical F-extensions (Proposition 12). The existence of solutions, which is guaranteed for F-extensions, therefore carries over to AP-extensions. Under the same assumptions, the AP-extensions are also equivalent with hyperrectangular overapproximations of F-extensions that have been used in qualitative simulations (Corollary 13). This has the advantage that the numerical analysis of PWL models can be preceded by the symbolic computation of equilibrium points and (in some cases) the analytic determination of their stability [72], as was done for the examples discussed in Section 6. More generally, the equivalency of the above-mentioned differential inclusions shows that the numerical method developed here is applicable for different solution concepts of PWL models proposed in the literature.

The practical usefulness of the approach was illustrated by means of the numerical analysis of three actual biological networks in synthetic biology. We developed PWL models for the circuits, either from scratch or by adapting existing ODE models, and parametrized the models with the help of literature data. For each of the models, we determined the equilibrium points and their stability, and we numerically computed solutions of the characteristic time-behavior of the networks. Although PWL

models are coarse-grained approximations of the actual biological processes taking place in the cell, and the dynamics of PWL models may differ from those of ODE models [73], even when steep sigmoid regulation functions are used [24,39], many of the observed dynamical properties of the synthetic networks could be reproduced by the simulations, such as the occurrence of stable oscillations in the repressilator (Section 6.1) and damped oscillations in the oscillator with positive feedback (Section 6.2).

The formulation of PWL models in the complementarity systems framework provides access to powerful numerical tools for the analysis of dynamic properties of naturally-occurring networks [9,10] or for the design of control schemes for synthetic networks [11]. Moreover, it also opens up the possibility to exploit results obtained for complementarity systems in the context of the analysis of PWL models. For example, as a first step in this direction, we showed in Section 5.1 that the strong monotonicity of the differential inclusion obtained after reformulating the PWL model as a MCS can be used to assure that an equilibrium point is (finite-time) stable.

Acknowledgments

Appendix. Alternative AP-extension of PWL models

As discussed in Section 3.1, the definition of AP-extensions could be relaxed by substituting different values $\sigma_j^k \in S^+(x_j, \theta_j^k)$ for the different occurrences of $s^+(x_j, \theta_j^k)$, and by decoupling the values for positive and negative step functions. This gives rise to an alternative AP-extension of the PWL model (1).

Definition 19 (*Alternative AP-extension of PWL models*)**.** The alternative AP-extension of a PWL model (1) is defined by the following differential inclusion

$$\dot{x} \in \begin{bmatrix} \hat{\mathbf{G}}_1(x) \\ \vdots \\ \hat{\mathbf{G}}_n(x) \end{bmatrix} = \begin{bmatrix} -\gamma_1 x_1 + \sum_{l \in L_1} \kappa_1^l \, \hat{b}_1^l(S) \\ \vdots \\ -\gamma_n x_n + \sum_{l \in L_n} \kappa_n^l \, \hat{b}_n^l(S) \end{bmatrix} \tag{A.1}$$

where $S = (S^+(x_1, \theta_1^1), \dots, S^+(x_1, \theta_1^{p_1}), \dots, S^+(x_n, \theta_n^1), \dots, S^+(x_n, \theta_n^{p_n}))^T$, and $\hat{b}_i^l(\cdot)$ is obtained from $b_i^l(\cdot)$, $i \in \{1, \dots, n\}$, by replacing every occurrence of $s^+(x_j, \theta_j^k)$ and $s^-(x_j, \theta_j^k)$ by $S^+(x_j, \theta_j^k)$ and $S^-(x_j, \theta_j^k)$, respectively.

This definition seems similar to Definition 8 but not equivalent, as shown in the example below. Consider the following simple PWL model:

$$\dot{x}_1 = -\gamma_1 x_1 + \kappa_1^1 s^-(x_1, \theta_1) + \kappa_1^2 s^+(x_1, \theta_1), \tag{A.2}$$

and let us assume that

$$0 < \kappa_1^1 < \gamma_1 \theta_1, \qquad 0 < \kappa_1^2 < \gamma_1 \theta_1, \quad \text{and}$$

$$\gamma_1 \theta_1 < \kappa_1^1 + \kappa_1^2. \tag{A.3}$$

The model (A.2) has three distinct regimes:

1. $x_1 < \kappa_1^1/\gamma_1$. Since $x_1 < \kappa_1^1/\gamma_1 < \theta_1$, the dynamical equation is given by:

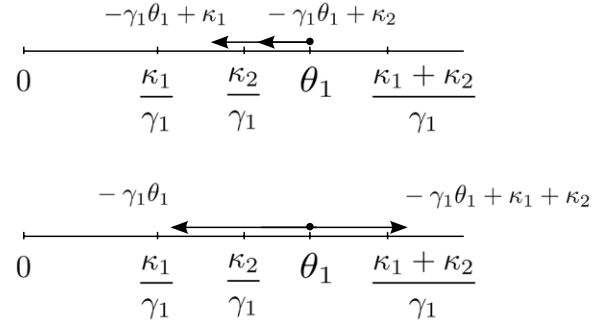$$\dot{x}_1 = -\gamma_1 x_1 + \kappa_1^1 > 0. \tag{A.4}$$

Fig. A.12. Right-hand side of two different extensions of the PWL model (A.2) at $x_1 = \theta_1$: the differential inclusion $\dot{x}_1 \in \mathbf{G}(x_1)$ (A.8), derived from Definition 8 (above) and the variant $\dot{x}_1 \in \hat{\mathbf{G}}(x_1)$ given by (A.10) (below).

2. $\kappa_1^1/\gamma_1 < x_1 < \theta_1$. The dynamical equation is given by:

$$\dot{x}_1 = -\gamma_1 x_1 + \kappa_1^1 < 0. \tag{A.5}$$

3. $\theta_1 < x_1$. The dynamical equation is given by:

$$\dot{x}_1 = -\gamma_1 x_1 + \kappa_1^2 < 0. \tag{A.6}$$

Notice that $x_1 = \theta_1$ is a discontinuity point of the system. In order to model the dynamics at this point, first consider the differential inclusion given by Definition 8:

$$\dot{x}_1 \in \mathbf{G}(x_1) = -\gamma_1 x_1 + \kappa_1^1 (1 - \sigma_1^1) + \kappa_1^2 \sigma_1^1, \tag{A.7}$$

with $\sigma_1^1 \in S^+(x_1, \theta_1)$. For $x_1 = \theta_1$, we obtain

$$\dot{x}_1 \in \mathbf{G}(x_1) = -\gamma_1 x_1 + \kappa_1^1(1 - \sigma_1^1) + \kappa_1^2 \sigma_1^1,$$

$$\text{with } \sigma_1^1 \in [0, 1]. \tag{A.8}$$

Under the assumption (A.3), it therefore holds that $\dot{x}_1 < 0$, as expected from the dynamics in the regions above and below $x_1 = \theta_1$ (see Fig. A.12). The point of discontinuity is a *crossing point* in the terminology of Filippov solutions. A quick analysis reveals that, when the differential inclusion is defined as in Definition 8, the system has a single equilibrium point $x_1 = \kappa_1^1/\gamma_1$.

Alternatively, following (A.1), the dynamics of the PWL model can be modeled by means of the differential inclusion

$$\dot{x}_1 \in \hat{\mathbf{G}}(x_1) = -\gamma_1 x_1 + \kappa_1^1 S^-(x_1, \theta_1) + \kappa_1^2 S^+(x_1, \theta_1). \tag{A.9}$$

At $x_1 = \theta_1$ this yields:

$$\dot{x}_1 \in \hat{\mathbf{G}}(x_1) = -\gamma_1 x_1 + \sigma, \quad \text{with } \sigma \in [0, \kappa_1^1 + \kappa_1^2]. \tag{A.10}$$

Note that (A.10) differs from (A.8), and that $0 \in \hat{\mathbf{G}}(x_1)$ since $\kappa_1^1 + \kappa_1^2 > \gamma_1 \theta_1$. This means that the differential inclusion (A.10) introduces an additional equilibrium point in θ_1 which is not a solution in the sense of Definition 8 (Fig. A.12). As explained in Section 3.1, we prefer Definition 8 above Definition 19.

References

[1] R. Hengge-Aronis, The general stress response in *Escherichia coli*, in: G. Storz, R. Hengge-Aronis (Eds.), Bacterial Stress Responses, ASM Press, Washington, DC, 2000, pp. 161–177.

[2] U. Alon, An Introduction to Systems Biology: Design Principles of Biological Circuits, Chapman & Hall/CRC, Boca Raton, FL, 2007.

[3] A.S. Khalil, J.J. Collins, Synthetic biology: applications come of age, Nat. Rev. Genet. 11 (5) (2010) 367–379.

[4] H. Bolouri, Computational Modeling of Gene Regulatory Networks — A Primer, Imperial College Press, London, 2008.

[5] G. Karlebach, R. Shamir, Modelling and analysis of gene regulatory networks, Nat. Rev. Mol. Cell Biol. 9 (10) (2008) 770–780.

[6] C. Chaouiya, A. Naldi, D. Thieffry, Logical modelling of gene regulatory networks with GINsim, in: J. van Helden, A. Toussaint, D. Thieffry (Eds.), Bacterial Molecular Networks: Methods and Protocols, in: Methods in Molecular Biology, vol. 804, Springer, New York, 2012, pp. 463–479.

[7] H. de Jong, D. Ropers, Strategies for dealing with incomplete information in the modeling of molecular interaction networks, Brief. Bioinform. 7 (4) (2006) 354–363.

[8] L. Glass, H.T. Siegelmann, Logical and symbolic analysis of robust biological dynamics, Curr. Opin. Genet. Dev. 20 (6) (2010) 644–649.

[9] W. Abou-Jaoude, M. Chaves, J.-L. Gouze, A theoretical exploration of birhythmicity in the p53-Mdm2 network, PLoS ONE 6 (2) (2011) e17075.

[10] L. Tournier, M. Chaves, Uncovering operational interactions in genetic networks using asynchronous Boolean dynamics, J. Theor. Biol. 260 (2) (2009) 196–209.

[11] R. Edwards, S. Kim, P. van den Driessche, Control design for sustained oscillation in a two gene regulatory network, J. Math. Biol. 62 (4) (2011) 453–479.

[12] L. Glass, S.A. Kauffman, The logical analysis of continuous non-linear biochemical control networks, J. Theor. Biol. 39 (1) (1973) 103–129.

[13] R. Casey, H. de Jong, J.-L. Gouzé, Piecewise-linear models of genetic regulatory networks: equilibria and their stability, J. Math. Biol. 52 (1) (2006) 27–56.

[14] R. Edwards, Analysis of continuous-time switching networks, Physica D 146 (1–4) (2000) 165–199.

[15] E. Farcot, J.-L. Gouzé, Periodic solutions of piecewise affine gene network models with non uniform decay rates: the case of a negative feedback loop, Acta Biotheor. 57 (4) (2009) 429–455.

[16] L. Glass, J.S. Pasternack, Stable oscillations in mathematical models of biological control systems, J. Math. Biol. 6 (1978) 207–223.

[17] A.F. Filippov, Differential Equations with Discontinuous Right Hand Sides, Kluwer, Dordrecht, The Netherlands, 1988.

[18] J.-L. Gouzé, T. Sari, A class of piecewise linear differential equations arising in biological models, Dyn. Syst. 17 (4) (2002) 299–316.

[19] A. Machina, A. Ponosov, Filippov solutions in the analysis of piecewise linear models describing gene regulatory networks, Nonlinear Anal. TMA 74 (3) (2011) 882–900.

[20] A. Machina, R. Edwards, P. van den Driessche, Singular dynamics in gene network models, SIAM J. Appl. Dyn. Syst. 12 (1) (2013) 95–125.

[21] G. Batt, B. Besson, P.E. Ciron, H. de Jong, E. Dumas, J. Geiselmann, R. Monte, P.T. Monteiro, M. Page, F. Rechenmann, D. Ropers, Genetic Network Analyzer: a tool for the qualitative modeling and simulation of bacterial regulatory networks, in: J. van Helden, A. Toussaint, D. Thieffry (Eds.), Bacterial Molecular Networks: Methods and Protocols, in: Methods in Molecular Biology, vol. 804, Springer, New York, 2012, pp. 439–462.

[22] G. Batt, H. de Jong, M. Page, J. Geiselmann, Symbolic reachability analysis of genetic regulatory networks using discrete abstractions, Automatica 44 (4) (2008) 982–989.

[23] L. Ironi, L. Panzeri, A computational framework for qualitative simulation of nonlinear dynamical models of gene-regulatory networks, BMC Bioinform. 10 (Suppl 12) (2009) S14.

[24] E. Plahte, S. Kjóglum, Analysis and generic properties of gene regulatory networks with graded response functions, Physica D 201 (1) (2005) 150–176.

[25] M.A. Aizerman, E.S. Pyatnitskii, Foundation of a theory of discontinuous systems. 1 & 2, Autom. Remote Control 35 (1974) 1066–1079 & 1066–1079.

[26] V. Acary, B. Brogliato, Numerical Methods for Nonsmooth Dynamical Systems. Applications in Mechanics and Electronics, in: Lecture Notes in Applied and Computational Mechanics, vol. 35, Springer, Berlin, 2008, p. 525. xxi.

[27] W.P.M.H. Heemels, J.M. Schumacher, S. Weiland, Linear complementarity systems, SIAM J. Appl. Math. 60 (2000) 1234–1269.

[28] J.-S. Pang, D. Stewart, Differential variational inequalities, Math. Program. A 113 (2) (2008).

[29] V. Acary, O. Bonnefon, B. Brogliato, Time-stepping numerical simulation of switched circuits with the nonsmooth dynamical systems approach, IEEE Trans. Comput.-aided Des. Integr. Circuits Syst. 29 (7) (2010) 1042–1055.

[30] M.B. Elowitz, S. Leibler, A synthetic oscillatory network of transcriptional regulators, Nature 403 (6767) (2000) 335–338.

[31] M.R. Atkinson, M.A. Savageau, J.T. Myers, A.J. Ninfa, Development of genetic circuitry exhibiting toggle switch or oscillatory behavior in *Escherichia coli*, Cell 113 (5) (2003) 597–608.

[32] I. Cantone, L. Marucci, F. Iorio, M.A. Ricci, V. Belcastro, M. Bansal, S. Santini, M. di Bernardo, D. di Bernardo, P.M. Cosma, A yeast synthetic network for *in vivo* assessment of reverse-engineering, Cell 137 (1) (2009) 172–181.

[33] H. de Jong, J.-L. Gouzé, C. Hernandez, M. Page, T. Sari, J. Geiselmann, Qualitative simulation of genetic regulatory networks using piecewise-linear models, Bull. Math. Biol. 66 (2) (2004) 301–340.

[34] T. Mestl, E. Plahte, S.W. Omholt, A mathematical framework for describing and analysing gene regulatory networks, J. Theor. Biol. 176 (2) (1995) 291–300.

[35] R. Thomas, R. d'Ari, Biological Feedback, CRC Press, Boca Raton, FL, 1990.

[36] G. Batt, M. Page, I. Cantone, G. Goessler, P.T. Monteiro, H. de Jong, Efficient parameter search for qualitative models of regulatory networks using symbolic model checking, Bioinform. 26 (18) (2010) i603–i610.

[37] Z. Kohavi, N.J. Jha, Switching and Finite Automata Theory, third ed., Cambridge University Press, 2010.

[38] E. Plahte, T. Mestl, S.W. Omholt, A methodological basis for description and analysis of systems with complex switch-like interactions, J. Math. Biol. 36 (4) (1998) 321–348.

[39] L. Ironi, L. Panzeri, E. Plahte, V. Simoncini, Dynamics of actively regulated gene networks, Physica D 240 (8) (2011) 779–794.

[40] A. Machina, A. Ponsonov, Stability of stationary solutions of piecewise affine differential equations describing gene regulatory networks, J. Math. Anal. Appl. 380 (2) (2011) 736–749.

[41] Y.V. Orlov, Discontinuous Systems, in: Communications and Control Engineering, Springer Verlag, 2009.

[42] V.I. Utkin, Variable structure systems with sliding modes: a survey, IEEE Trans. Automat. Control 22 (1977) 212–222.

[43] V.I. Utkin, Sliding Modes in Control Optimization, Springer Verlag, Berlin, Berlin, 1992.

[44] V. Acary, O. Bonnefon, B. Brogliato, Nonsmooth Modeling and Simulation for Switched Circuits, in: Lecture Notes in Electrical Engineering, vol. 69, Dordrecht, Springer, 2011, p. 284. xxiii.

[45] V. Acary, B. Brogliato, Implicit Euler numerical scheme and chattering-free implementation of sliding mode systems, Syst. Control Lett. 59 (5) (2010) 284–293.

[46] F. Facchinei, J.S. Pang, Finite-dimensional Variational Inequalities and Complementarity Problems, Volume I & II, in: Springer Series in Operations Research, Springer Verlag NY. Inc., 2003.

[47] J.B. Hiriart-Urruty, C. Lemaréchal, Fundamentals of Convex Analysis, Springer Verlag, 2001.

[48] R.T. Rockafellar, R.J.B. Wets, Variational Analysis, Vol. 317, Springer Verlag, New York, 1998.

[49] S.C. Billups, Algorithms for Complementarity Problems and Generalized Equations. Ph.D. thesis, University of Wisconsin, Madison, available as Technical Report MP-TR-1995-14, 1995.

[50] S.C. Billups, S.P. Dirkse, M.C. Ferris, A comparison of large scale mixed complementarity problem solvers, Comput. Optim. Appl. 7 (1997) 3–25.

[51] S.P. Dirkse, M.C. Ferris, The PATH solver: a non-monotone stabilization scheme for mixed complementarity problems, Optim. Methods Softw. 5 (1995) 123–156.

[52] M.C. Ferris, T.S. Munson, Interfaces to PATH 3.0: Design, implementation and usage, Comput. Optim. Appl. 12 (1–3) (1999) 207–227.

[53] B. Brogliato, A. Daniilidis, C. Lemaréchal, V. Acary, On the equivalence between complementarity systems, projected systems and differential inclusions, Syst. Control Lett. 55 (2006) 45–51.

[54] C. Georgescu, B. Brogliato, V. Acary, Switching, relay and complementarity systems: a tutorial on their well-posedness and relationships, Physica D 241 (22) (2012) 1985–2002.

[55] D. Stewart, A high accuracy method for solving ODEs with discontinuous right-hand-side, Numer. Math. 58 (1990) 299–328.

[56] A.L. Dontchev, F. Lempio, Difference methods for differential inclusions: a survey, SIAM Reviews 34 (2) (1992) 263–294.

[57] V. Acary, B. Brogliato, D. Goeleven, Higher order Moreau's sweeping process: mathematical formulation and numerical simulation, Math. Program. Ser. A 113 (2008) 133–217.

[58] M.K. Camlibel, W.P.M.H. Heemels, J.M. Schumacher, Consistency of a time-stepping method for a class of piecewise-linear networks, IEEE Trans. Circuits Syst. I. 49 (2002) 349–357.

[59] L. Han, A. Tiwari, K. Camlibel, J.S. Pang, Convergence of time-stepping schemes for passive and extended linear complementarity systems, SIAM J. Numer. Anal. 47 (5) (2009) 3768–3796.

[60] N.H. Josephy, Newton's Method for Generalized Equations, Technical report, Mathematics Research Center, University of Wisconsin, Madison, 1979.

[61] T. Rutherford, Miles: A Mixed Inequality and Nonlinear Equation Solver, 1993.

[62] R.W. Cottle, J. Pang, R.E. Stone, The Linear Complementarity Problem, Academic Press, Inc., Boston, MA, 1992.

[63] Faiz A. Al-Khayyal, An implicit enumeration procedure for the general linear complementarity problem, Math. Program. Study 31 (1987) 1–20.

[64] J. Júdice, A. Faustino, I. Ribeiro, On the solution of NP-hard linear complementarity problems, TOP 10 (2002) 125–145. http://dx.doi.org/10.1007/BF02578944.

[65] H.D. Sherali, R.S. Krishnamurthy, F.A. Al-Khayyal, Enumeration approach for linear complementarity problems based on a reformulation-linearization technique, J. Optim. Theory Appl. 99 (2) (1998) 481–507.

[66] V. Acary, F. Pérignon, An Introduction to Siconos, Technical Report TR-0340, INRIA, 2007, http://hal.inria.fr/inria-00162911/en/.

[67] B. Brogliato, Absolute stability and the Lagrange–Dirichlet theorem with monotone multivalued mappings, Syst. Control Lett. 51 (5) (2004) 343–353.

[68] V. Acary, B. Brogliato, Y.V. Orlov, Chattering-free digital sliding-mode control with state observer and disturbance rejection, IEEE Trans. Automat. Control 57 (5) (2012) 1087–1101.

[69] O. Purcell, N.J. Savery, C.S. Grierson, M. di Bernardo, A comparative analysis of synthetic genetic oscillators, J. R. Soc. Interface 7 (52) (2010) 1503–1524.

[70] J.J. Tyson, H.G. Othmer, The dynamics of feedback control circuits in biochemical pathways, Progr. Theor. Biol. 5 (1978) 1–62.

[71] L. Marucci, D.A.W. Barton, I. Cantone, M.A. Ricci, M.P. Cosma, S. Santini, D. di Bernardo, M. di Bernardo, How to turn a genetic circuit into a synthetic tunable oscillator, or a bistable switch, PLoS ONE 4 (12) (2011) E8083.

[72] H. de Jong, M. Page, Search for steady states of piecewise-linear differential equation models of genetic regulatory networks, ACM/IEEE Trans. Comput. Biol. Bioinform. 5 (2) (2008) 208–222.

[73] A. Polynikis, S.J. Hogan, M. di Bernardo, Comparing different ODE modelling approaches for gene regulatory networks, J. Theor. Biol. 261 (4) (2009) 511–530.